JHEP

Published for SISSA by Springer

Received: November 17, 2017
Revised: January 9, 2018
Accepted: January 24, 2018
Published: February 6, 2018

Large NLO corrections in $t\bar{t}W^{\pm}$ and $t\bar{t}t\bar{t}$ hadroproduction from supposedly subleading EW contributions

Rikkert Frederix,[a] **Davide Pagani**[a] **and Marco Zaro**[b,c,d]

[a] *Technische Universität München,*
James-Franck-Str. 1, D-85748 Garching, Germany
[b] *Nikhef,*
Science Park 105, NL-1098 XG Amsterdam, The Netherlands
[c] *Sorbonne Universités, UPMC Univ. Paris 06, UMR 7589, LPTHE,*
F-75005, Paris, France
[d] *CNRS, UMR 7589, LPTHE,*
F-75005, Paris, France

E-mail: rikkert.frederix@tum.de, davide.pagani@tum.de, m.zaro@nikhef.nl

Abstract: We calculate the complete-NLO predictions for $t\bar{t}W^{\pm}$ and $t\bar{t}t\bar{t}$ production in proton-proton collisions at 13 and 100 TeV. All the non-vanishing contributions of $\mathcal{O}(\alpha_s^i\alpha^j)$ with $i+j=3,4$ for $t\bar{t}W^{\pm}$ and $i+j=4,5$ for $t\bar{t}t\bar{t}$ are evaluated without any approximation. For $t\bar{t}W^{\pm}$ we find that, due to the presence of $tW \to tW$ scattering, at 13(100) TeV the $\mathcal{O}(\alpha_s\alpha^3)$ contribution is about 12(70)% of the LO, i.e., it is larger than the so-called NLO EW corrections (the $\mathcal{O}(\alpha_s^2\alpha^2)$ terms) and has opposite sign. In the case of $t\bar{t}t\bar{t}$ production, large contributions from electroweak $tt \to tt$ scattering are already present at LO in the $\mathcal{O}(\alpha_s^3\alpha)$ and $\mathcal{O}(\alpha_s^2\alpha^2)$ terms. For the same reason we find that both NLO terms of $\mathcal{O}(\alpha_s^4\alpha)$, i.e., the NLO EW corrections, and $\mathcal{O}(\alpha_s^3\alpha^2)$ are large ($\pm 15\%$ of the LO) and their relative contributions strongly depend on the values of the renormalisation and factorisation scales. However, large accidental cancellations are present (away from the threshold region) between these two contributions. Moreover, the NLO corrections strongly depend on the kinematics and are particularly large at the threshold, where even the relative contribution from $\mathcal{O}(\alpha_s^2\alpha^3)$ terms amounts to tens of percents.

Keywords: NLO Computations, QCD Phenomenology

ArXiv ePrint: 1711.02116

https://doi.org/10.1007/JHEP02(2018)031

JHEP02(2018)031

Contents

1 Introduction

Precise predictions for Standard-Model (SM) processes at high-energy colliders are an essential ingredient for a correct and reliable comparison between experimental data and theories describing the fundamental interactions of Nature. At the LHC and future colliders, the capability of performing further consistency checks for the SM as well as the possibility of identifying beyond-the-Standard-Model (BSM) effects critically depend on the size of the theory uncertainties.

At high-energies, SM calculations can be performed in a perturbative approach. Thus, the precision of the prediction for a generic observable can be successively improved by taking into account higher-order effects. In particular, the so-called fixed-order calculations consist in the perturbative expansion in powers of the two SM parameters α_s and α. The former parametrises strong interactions and its value is roughly 0.1 at the TeV scale or at the typical energy scales involved at the LHC. The latter parametrises electroweak (EW) interactions and its value is roughly 0.01. On the other hand, EW interactions also depend on the mass of the W and Z bosons (or alternatively on any other three independent parameters for the EW gauge sector) and the masses of the fermions and the Higgs boson.

Typically, the leading-order (LO) contribution for a specific process is given by the first non-vanishing terms of $\mathcal{O}(\alpha_s^i \alpha^j)$, i.e., those with the smallest value for $i+j$ and the largest value of i. For this reason, "LO prediction" in general refers to this level of accuracy, which is not sufficiently precise for almost all processes at the LHC. The calculation of next-to-LO (NLO) predictions in QCD, which consists in the inclusion of $\mathcal{O}(\alpha_s^{i+1} \alpha^j)$ terms, can be performed automatically and with publicly available tools [1–13] for most of the processes. Recently, also NLO EW corrections, which consist of $\mathcal{O}(\alpha_s^i \alpha^{j+1})$ terms, have been calculated via (semi-)automated tools [5–7, 11, 14–21] for a large variety of processes.

Being $\alpha < \alpha_s$, NLO EW corrections are typically smaller than NLO QCD corrections at the inclusive level, but they can be considerably enhanced at the differential level due

JHEP02(2018)031

to different kinds of effects such as weak Sudakov enhancements or collinear photon final-state-radiation (FSR) in sufficiently exclusive observables. Thus, they have to be taken into account for a reliable comparison to data. For many production processes at the LHC, also next-to-NLO (NNLO) QCD corrections, the $\mathcal{O}(\alpha_s^{i+2}\alpha^j)$ contributions, are essential and indeed many calculations have appeared in the recent years (see, e.g., ref. [22] and references therein). Even the next-to-NNLO ($\mathrm{N^3LO}$) QCD calculation for the Higgs production cross section is now available [23, 24].

From a technical point of view, NLO QCD and EW corrections are simpler than NNLO corrections; they involve at most one loop or one additional radiated parton more than the LO calculation. However, they are not the only perturbative orders sharing this feature. Already starting from $2 \to 2$ processes with coloured and EW-charged initial- and final-state particles, such as dijet or top-quark pair hadroproduction, additional NLO terms appears. For these two processes, one-loop and real-emission corrections in the SM involve also $\mathcal{O}(\alpha_s\alpha^2)$ and $\mathcal{O}(\alpha^3)$ terms, which are neither part of the NLO QCD corrections nor of the NLO EW ones. Moreover, Born diagrams originate also $\mathcal{O}(\alpha_s\alpha)$ and $\mathcal{O}(\alpha^2)$ contributions, which are typically not included in LO predictions. The sum of all these contributions yields the prediction at "complete-NLO" accuracy.

The complete-NLO results for dijet production at the LHC have been calculated in ref. [19] and for top-quark pair production in ref. [25], the latter also combined with NNLO QCD corrections. Although one-loop contributions that are not part of NLO QCD and NLO EW corrections are present for many production processes at the LHC, calculations at this level of accuracy are rare, and those performed for dijet and top-quark pair production represent an exception. The reason is twofold. First, being higher-order effects and $\alpha/\alpha_s \sim 0.1$ these corrections are expected to be smaller than standard NLO EW ones, and indeed they are for the case of dijet and top-quark pair production. Second, only with the recent automation of the calculation of EW corrections the necessary effort for calculating these additional orders has been reduced and therefore justified given their expected smallness. Besides these reasons, in the subleading orders there can be new production mechanisms and care has to be taken to avoid process overlap. For example, the $\mathcal{O}(\alpha^2)$ contribution to dijet production contains hadronically decaying heavy vector bosons.

To our knowledge, the only other calculation where all the NLO effects beyond the NLO QCD and NLO EW accuracy have been considered is the case of vector-boson-scattering (VBS) for two positively charged W bosons at the LHC including leptonic decays, namely the $pp \to \mu^+\nu_\mu e^+\nu_e jj$ process [26]. This complete-NLO prediction includes all the terms of $\mathcal{O}(\alpha_s^i\alpha^j)$ with $i+j = 6, 7$ and $j \geq 4$, featuring both QCD-induced W^+W^+jj production and electroweak W^+W^+ scattering. Remarkably, at variance with dijet and top-quark pair production, the expected hierarchy of the different perturbative orders is not respected. Indeed, with proper VBS cuts the $\mathcal{O}(\alpha^7)$ is by far the largest of the NLO contributions and moreover $\mathcal{O}(\alpha^7) > \mathcal{O}(\alpha^6\alpha_s) > \mathcal{O}(\alpha^5\alpha_s^2) \sim \mathcal{O}(\alpha^4\alpha_s^3)$.

In this article we want to give evidence that what has been found in ref. [26], i.e., large contributions from supposedly subleading corrections, is not an exception due to the particularities of this process [27] and standard VBS selection cuts, which reduce the "QCD backgrounds". It is rather a feature that may appear whenever the process considered

JHEP02(2018)031

involves the scattering of heavy particles in the SM, namely the W, Z and Higgs bosons, but also top quarks. Indeed, although it is customary to expand in powers of α, for these kind of processes $\mathcal{O}(\alpha)$ corrections actually involve enhancements already at the coupling level, e.g., in the interactions among the top-quark, the Higgs boson and the longitudinal polarisations of the W and Z bosons. Thus, the $\mathcal{O}(\alpha) \sim 0.01$ assumption is in general not valid and the expected hierarchy among perturbative orders may be not respected even at the inclusive level.

Here we focus on the case of the top quark and we explicitly show two different cases in which the expected hierarchy is not respected: the $t\bar{t}W^{\pm}$ and $t\bar{t}t\bar{t}$ production processes, which are already part of the current physics program at the LHC [28–30]. To this purpose we perform the calculation of the complete-NLO predictions of these two processes at 13 and 100 TeV in proton-proton collisions. All the seven $\mathcal{O}(\alpha_s^i\alpha^j)$ contributions with $i+j = 3,4$ and $j \geq 1$ for $t\bar{t}W^{\pm}$ production and all the eleven $\mathcal{O}(\alpha_s^i\alpha^j)$ contributions with $i+j = 4,5$ are calculated exactly without any approximation. For both processes the calculation has been performed in a completely automated way via an extension of the code MadGraph5_aMC@NLO [11]. This extension has already been validated for the NLO EW case in refs. [18, 31] and in refs. [19, 25] for the calculation of the complete-NLO corrections. The code will soon be released and further documented in a detailed dedicated paper [32].

Complete-NLO corrections involve large contributions for both the $t\bar{t}W^{\pm}$ and $t\bar{t}t\bar{t}$ production processes, but very different structures underlie the two calculations. Indeed, while large EW effects in $t\bar{t}W^{\pm}$ production originate from the $tW \to tW$ scattering, which appears only via NLO corrections, in $t\bar{t}t\bar{t}$ production large EW effects are already present at LO, due to the electroweak $tt \to tt$ scattering.

It has been noted in ref. [33] that EW $pp \to t\bar{t}W^{\pm}j$ production involves $tW \to tW$ scattering via the $gq \to t\bar{t}W^{\pm}q'$ channel. Even though ref. [33] focusses on BSM physics in $tW \to tW$ scattering, this contribution is sizeable already in the SM and is part of the NLO contributions of $\mathcal{O}(\alpha_s\alpha^3)$ to the inclusive $t\bar{t}W^{\pm}$ production. It is *not* part of the NLO EW corrections, which are of $\mathcal{O}(\alpha_s^2\alpha^2)$ and have already been calculated in ref. [18]. However, while in the case of $pp \to t\bar{t}W^{\pm}j$ production the final-state jet must be reconstructed, this is not necessary for the inclusive $pp \to t\bar{t}W^{\pm}$ process. In fact, we will argue that the $tW \to tW$ scattering component can be enhanced over the irreducible background from inclusive $t\bar{t}W^{\pm}$ production by applying a central jet veto.

Recently it was suggested that $t\bar{t}t\bar{t}$ production can be used as a probe of the top-quark Yukawa coupling (y_t), as discussed in the tree-level analysis presented in ref. [34]. Performing an expansion in power of y_t one finds that $\mathcal{O}(y_t^2)$ and $\mathcal{O}(y_t^4)$ contributions to $t\bar{t}t\bar{t}$ production are not much smaller than purely-QCD induced terms (and in general non-Yukawa induced contributions) and therefore $t\bar{t}t\bar{t}$ production is quite sensitive to the value of the top Yukawa coupling. Expanding the LO prediction in powers of α, the $\mathcal{O}(y_t^2)$ and $\mathcal{O}(y_t^4)$ terms are fully included in the $\mathcal{O}(\alpha_s^3\alpha)$ and $\mathcal{O}(\alpha_s^2\alpha^2)$ terms. These perturbative orders are even larger than their Yukawa-induced components, and they also feature large cancellations at the inclusive level. It is therefore interesting to compute NLO corrections to all these terms, since we expect them to be large as well. Indeed, we find that they are much larger than the values expected from a naive α_s and α power counting. On the other hand, even larger cancellations are present among NLO terms, although not over the whole phase space.

JHEP02(2018)031

The structure of the paper is the following. In section 2 we describe the calculations and we introduce a more suitable notation for referring to the various $\mathcal{O}(\alpha_s^i\alpha^j)$ contributions. In section 3 we provide numerical results at the inclusive and differential levels for complete-NLO predictions for proton-proton collisions at 13 and 100 TeV. We discuss in detail the impact of the individual $\mathcal{O}(\alpha_s^i\alpha^j)$ contributions. The common input parameters are described in section 3.1, while $pp \to t\bar{t}W^\pm$ and $pp \to t\bar{t}t\bar{t}$ results are described in sections 3.2 and 3.3, respectively. Conclusions are given in section 4.

2 Calculation framework for $t\bar{t}W^\pm$ and $t\bar{t}t\bar{t}$ production at complete-NLO

Performing an expansion in powers of α_s and α, a generic observable for the processes $pp \to t\bar{t}W^\pm(+X)$ and $pp \to t\bar{t}t\bar{t}(+X)$ can be expressed as

$$\Sigma^{t\bar{t}W^\pm}(\alpha_s,\alpha) = \sum_{m+n\geq 2} \alpha_s^m \alpha^{n+1} \Sigma^{t\bar{t}W^\pm}_{m+n+1,n}\,, \tag{2.1}$$

$$\Sigma^{t\bar{t}t\bar{t}}(\alpha_s,\alpha) = \sum_{m+n\geq 4} \alpha_s^m \alpha^{n} \Sigma^{t\bar{t}t\bar{t}}_{m+n,n}\,, \tag{2.2}$$

respectively, where m and n are positive integer numbers and we have used the notation introduced in refs. [11, 17]. For $t\bar{t}W^\pm$ production, LO contributions consist of $\Sigma^{t\bar{t}W^\pm}_{m+n+1,n}$ terms with $m+n=2$ and are induced by tree-level diagrams only. NLO corrections are given by the terms with $m+n=3$ and are induced by the interference of diagrams from the all the possible Born-level and one-loop amplitudes as well all the possible interferences among tree-level diagrams involving one additional quark, gluon or photon emission. Analogously, for $t\bar{t}t\bar{t}$ production, LO contributions consist of $\Sigma^{t\bar{t}t\bar{t}}_{m+n,n}$ terms with $m+n=4$ and NLO corrections are given by the terms with $m+n=5$. In this work we calculate all the perturbative orders entering at the complete-NLO accuracy, i.e., $m+n=2,3$ for $\Sigma^{t\bar{t}W^\pm}(\alpha_s,\alpha)$ and $m+n=4,5$ for $\Sigma^{t\bar{t}t\bar{t}}(\alpha_s,\alpha)$.

Similarly to ref. [19], we introduce a more user-friendly notation for referring to the different $\Sigma^{t\bar{t}W^\pm}_{m+n+1,n}$ and $\Sigma^{t\bar{t}t\bar{t}}_{m+n,n}$ quantities. At LO accuracy, we can denote the $t\bar{t}W^\pm$ and $t\bar{t}t\bar{t}$ observables as $\Sigma^{t\bar{t}W^\pm}_{\rm LO}$ and $\Sigma^{t\bar{t}t\bar{t}}_{\rm LO}$ and further redefine the perturbative orders entering these two quantities as

$$\begin{aligned}\Sigma^{t\bar{t}W^\pm}_{\rm LO}(\alpha_s,\alpha) &= \alpha_s^2\alpha\Sigma^{t\bar{t}W^\pm}_{3,0} + \alpha_s\alpha\Sigma^{t\bar{t}W^\pm}_{3,1} + \alpha^2\Sigma^{t\bar{t}W^\pm}_{3,2} \\ &\equiv \Sigma_{\rm LO_1} + \Sigma_{\rm LO_2} + \Sigma_{\rm LO_3}\,, \end{aligned}\tag{2.3}$$

$$\begin{aligned}\Sigma^{t\bar{t}t\bar{t}}_{\rm LO}(\alpha_s,\alpha) &= \alpha_s^4\Sigma^{t\bar{t}t\bar{t}}_{4,0} + \alpha_s^3\alpha\Sigma^{t\bar{t}t\bar{t}}_{4,1} + \alpha_s^2\alpha^2\Sigma^{t\bar{t}t\bar{t}}_{4,2} + \alpha_s^3\alpha\Sigma^{t\bar{t}t\bar{t}}_{4,3} + \alpha^4\Sigma^{t\bar{t}t\bar{t}}_{4,4} \\ &\equiv \Sigma_{\rm LO_1} + \Sigma_{\rm LO_2} + \Sigma_{\rm LO_3} + \Sigma_{\rm LO_4} + \Sigma_{\rm LO_5}\,. \end{aligned}\tag{2.4}$$

In a similar fashion the NLO corrections and their single perturbative orders can be defined as

$$\begin{aligned}\Sigma^{t\bar{t}W^\pm}_{\rm NLO}(\alpha_s,\alpha) &= \alpha_s^3\alpha\Sigma^{t\bar{t}W^\pm}_{4,0} + \alpha_s^2\alpha^2\Sigma^{t\bar{t}W^\pm}_{4,1} + \alpha_s\alpha^3\Sigma^{t\bar{t}W^\pm}_{4,2} + \alpha^4\Sigma^{t\bar{t}W^\pm}_{4,3} \\ &\equiv \Sigma_{\rm NLO_1} + \Sigma_{\rm NLO_2} + \Sigma_{\rm NLO_3} + \Sigma_{\rm NLO_4}\,, \end{aligned}\tag{2.5}$$

$$\begin{aligned}\Sigma^{t\bar{t}t\bar{t}}_{\rm NLO}(\alpha_s,\alpha) &= \alpha_s^5\Sigma^{t\bar{t}t\bar{t}}_{5,0} + \alpha_s^4\alpha^1\Sigma^{t\bar{t}t\bar{t}}_{5,1} + \alpha_s^3\alpha^2\Sigma^{t\bar{t}t\bar{t}}_{5,2} + \alpha_s^2\alpha^3\Sigma^{t\bar{t}t\bar{t}}_{5,3} + \alpha_s^1\alpha^4\Sigma^{t\bar{t}t\bar{t}}_{5,4} + \alpha^5\Sigma^{t\bar{t}t\bar{t}}_{5,5} \\ &\equiv \Sigma_{\rm NLO_1} + \Sigma_{\rm NLO_2} + \Sigma_{\rm NLO_3} + \Sigma_{\rm NLO_4} + \Sigma_{\rm NLO_5} + \Sigma_{\rm NLO_6}\,. \end{aligned}\tag{2.6}$$

JHEP02(2018)031

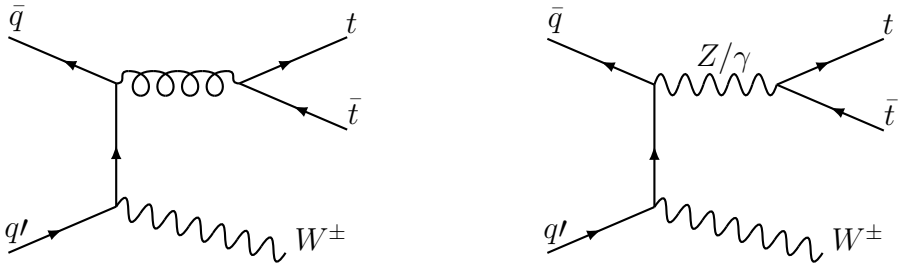

Figure 1. Representative diagrams for the Born $\bar{q}q' \to t\bar{t}W^{\pm}$ amplitude. The left diagram is of $\mathcal{O}(\alpha_s\alpha^{1/2})$, the right one is of $\mathcal{O}(\alpha^{3/2})$.

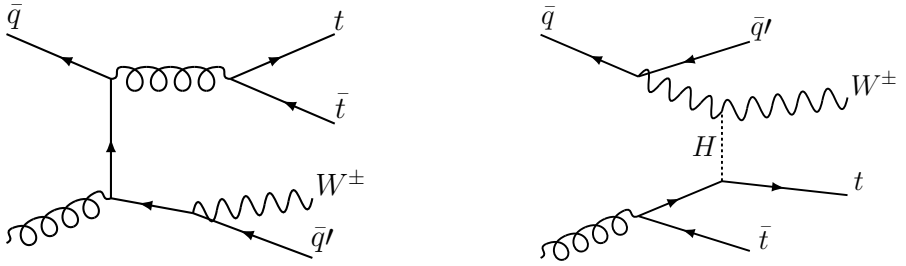

Figure 2. Representative diagrams for the $\bar{q}g \to t\bar{t}W^{\pm}\bar{q}'$ real-emission amplitudes. The left diagram is of $\mathcal{O}(\alpha_s^{3/2}\alpha^{1/2})$ and leads to $\log^2(p_T^2(t\bar{t})/m_W^2)$ terms in the NLO_1 contribution. The right one is of $\mathcal{O}(\alpha_s^{1/2}\alpha^{3/2})$, involves the $tW \to tW$ scattering and contributes to the NLO_3.

In the following we will use the symbols $\Sigma_{(\mathrm{N})\mathrm{LO}_i}$ or interchangeably their shortened aliases $(\mathrm{N})\mathrm{LO}_i$ for referring to the different perturbative orders. Clearly the $\Sigma_{(\mathrm{N})\mathrm{LO}_i}$ terms in $t\bar{t}W^{\pm}$ production, eqs. (2.3) and (2.5), and in $t\bar{t}t\bar{t}$ production, eqs. (2.4) and (2.6), are different quantities. One should bear in mind that, usually, with the term "LO" one refers only to LO_1, which here we will also denote as $\mathrm{LO}_{\mathrm{QCD}}$, while an observable at NLO QCD accuracy is $\Sigma_{\mathrm{LO}_1} + \Sigma_{\mathrm{NLO}_1}$, which we will also denote as $\mathrm{LO}_{\mathrm{QCD}} + \mathrm{NLO}_{\mathrm{QCD}}$. The so-called NLO EW corrections which are of $\mathcal{O}(\alpha)$ w.r.t. the LO_1, are the Σ_{NLO_2} terms, so we will also denote it as $\mathrm{NLO}_{\mathrm{EW}}$. Since in this article we will use the $(\mathrm{N})\mathrm{LO}_i$ notation, the term "LO" will refer to the sum of all the LO_i contributions rather than LO_1 alone. The prediction at complete-NLO accuracy, which is the sum of all the LO_i and NLO_i terms, will be also denoted as "LO + NLO".

We now turn to the description of the structures underlying the calculation of $t\bar{t}W^{\pm}$ and $t\bar{t}t\bar{t}$ predictions at complete-NLO accuracy. We start with $t\bar{t}W^{\pm}$ production, which is in turn composed by $t\bar{t}W^{+}$ and $t\bar{t}W^{-}$ production, and then we move to $t\bar{t}t\bar{t}$ production.

In $t\bar{t}W^{+}(t\bar{t}W^{-})$production, tree-level diagrams originate only from $u\bar{d}(\bar{u}d)$ initial states (u and d denote generic up- and down-type quarks), where a $W^{+}(W^{-})$ is radiated from the $u(d)$ quark and the $t\bar{t}$ pair is produced either via a gluon or a photon/Z boson (see figure 1). The former class of diagrams leads to the LO_1 via squared amplitude, the latter to LO_3. The interference between these two classes of diagrams is absent due to colour, thus LO_2 is analytically zero. Conversely, all the NLO_i contributions are non-vanishing.

JHEP02(2018)031

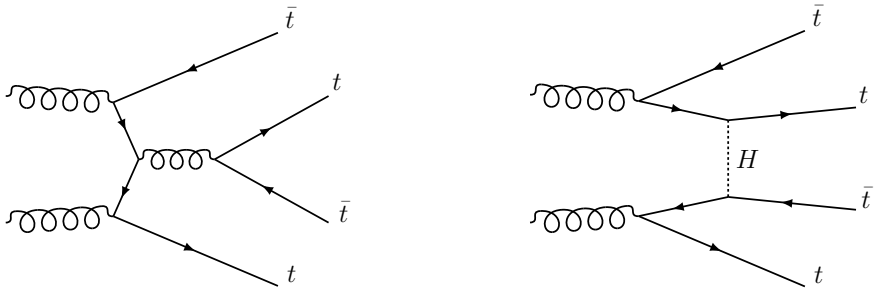

Figure 3. Representative diagrams for the Born $gg \to t\bar{t}t\bar{t}$ amplitude. The left diagram is of $\mathcal{O}(\alpha_s^2)$, the right one is of $\mathcal{O}(\alpha_s\alpha)$. Both diagrams involve $tt \to tt$ scattering contributions.

The NLO_1 is in general large, it has been calculated in refs. [10, 35–37] and studied in detail in ref. [38], where giant K-factors for the $p_T(t\bar{t})$ distribution have been found. Large QCD corrections are induced also by the opening of the $gq \to t\bar{t}W^{\pm}q'$ channels, which depend on the gluon luminosity and are therefore enhanced for high-energy proton-proton collisions. Moreover, the $p_T(t\bar{t})$ distribution receives an additional $\log^2(p_T^2(t\bar{t})/m_W^2)$ enhancement in the qg initial-state subprocess (see left diagram in figure 2 and ref. [38] for a detailed discussion). Also, the impact of soft-gluon emissions is non-negligible and their resummed contribution has been calculated in refs. [39–41] up to next-to-next-to-leading-logarithmic accuracy. The NLO_2 has been calculated for the first time in ref. [18] and further phenomenological studies have been provided in ref. [42]. In a boosted regime, due to Sudakov logarithms, the NLO_2 contribution can be as large as the NLO QCD scale uncertainty.

The NLO_3 and NLO_4 contributions are calculated for the first time here. In particular, the NLO_3 contribution is expected to be sizeable since it contains $gq \to t\bar{t}W^{\pm}q'$ real-emission channels that involve EW $tW \to tW$ scattering (see right diagram in figure 2), which as pointed out in ref. [33] can be quite large. Moreover, as in the case of NLO_1, due to the initial-state gluon this channel becomes even larger by increasing the energy of proton-proton collisions.[1] The $tW \to tW$ scattering is present also in the NLO_4 via the $\gamma q \to t\bar{t}W^{\pm}q'$, however in this case its contribution is suppressed by a factor α/α_s and especially by the smaller luminosity of the photon. In addition to the real radiation of quarks, also the $q\bar{q}' \to t\bar{t}W^{\pm}g$ and $q\bar{q}' \to t\bar{t}W^{\pm}\gamma$ processes contribute to the NLO_3 and NLO_4, respectively. Concerning virtual corrections, the NLO_4 receives contributions only from one-loop amplitudes of $\mathcal{O}(\alpha^{5/2})$, interfering with $\mathcal{O}(\alpha^{3/2})$ Born diagrams. Instead, the NLO_3 receives contributions both from $\mathcal{O}(\alpha^{5/2})$ and $\mathcal{O}(\alpha_s\alpha^{3/2})$ one-loop amplitudes interfering with $\mathcal{O}(\alpha_s\alpha^{1/2})$ and $\mathcal{O}(\alpha^{3/2})$ Born diagrams, respectively. Clearly, due to the different charges, NLO_i terms are different for the $t\bar{t}W^+$ and $t\bar{t}W^-$ case, however, since we did not find large qualitative differences at the numerical level, we provide only inclusive results for $t\bar{t}W^{\pm}$ production.

[1] In $t\bar{t}Z(t\bar{t}H)$ production the NLO_3 contributions feature $tH \to tH(tZ \to tZ)$ scattering in $gq \to t\bar{t}Zq(gq \to t\bar{t}Hq)$ real-emission channels. However, at variance with $t\bar{t}W^{\pm}$ production, the gg initial state is available at LO_{QCD}. Thus, the qg luminosity is not giving an enhancement and the relative impact from NLO_3 is smaller than in $t\bar{t}W^{\pm}$ production.

JHEP02(2018)031

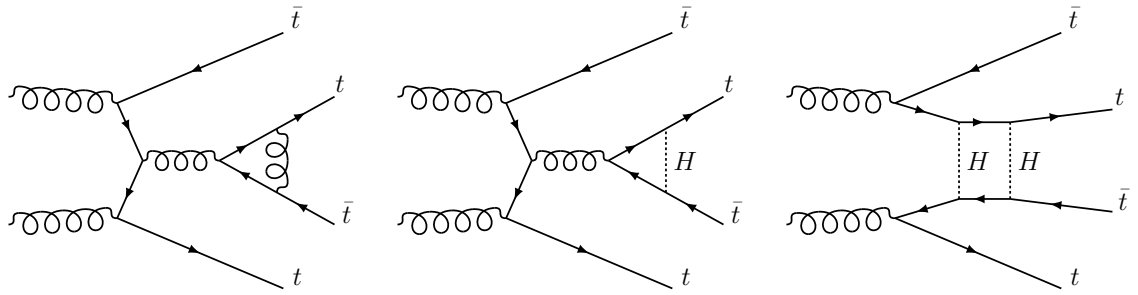

Figure 4. Representative diagrams for the one-loop $gg \to t\bar{t}t\bar{t}$ amplitude. The left diagram is of $\mathcal{O}(\alpha_s^3)$, the central one is of $\mathcal{O}(\alpha_s^2\alpha)$ and the right one is of $\mathcal{O}(\alpha_s\alpha^2)$. The interferences of these diagrams with those shown in figure 3 lead to contributions to NLO_1, NLO_2, NLO_3 and NLO_4.

We now turn to the case of $t\bar{t}t\bar{t}$ production, whose calculation involves a much higher level of complexity. While the NLO_1 contribution have already been calculated in refs. [11, 43] and studied in detail in ref. [38], all the other $(\text{N})\text{LO}_i$ contributions are calculated for the first time here.

The $gg \to t\bar{t}t\bar{t}$ Born amplitude contains only $\mathcal{O}(\alpha_s^2)$ and $\mathcal{O}(\alpha_s\alpha)$ diagrams, while the $q\bar{q} \to t\bar{t}t\bar{t}$ Born amplitude contains also $\mathcal{O}(\alpha^2)$ diagrams. Thus the gg initial state contributes to LO_i with $i \leq 3$ and the $q\bar{q}$ initial states contribute to all the LO_i. Also the γg and $\gamma\gamma$ initial states are available at the Born level; they contributes to LO_i with respectively $i \geq 2$ and $i \geq 3$. However, their contributions are suppressed by the size of the photon parton distribution function (PDF). Representative $gg \to t\bar{t}t\bar{t}$ Born diagrams are shown in figure 3. As already mentioned in the introduction, LO_2 and LO_3 are larger than the values naively expected from α_s and α power counting, i.e., $\text{LO}_2 \gg (\alpha/\alpha_s) \times \text{LO}_{\text{QCD}}$ and $\text{LO}_3 \gg (\alpha/\alpha_s)^2 \times \text{LO}_{\text{QCD}}$. Thus, NLO_2, NLO_3 and also NLO_4 are expected to be non-negligible, especially NLO_2, NLO_3 because they involve "QCD corrections"[2] to LO_2 and LO_3 contributions, respectively. As discussed in ref. [38], the $t\bar{t}t\bar{t}$ production cross-section is mainly given by the gg initial state, for this reason we expect LO_4, $(\text{N})\text{LO}_5$ and NLO_6 to be negligible. Representative $gg \to t\bar{t}t\bar{t}$ one-loop diagrams are shown in figure 4. Although suppressed by the photon luminosity, also the γg and $\gamma\gamma$ initial states contribute to NLO_i with $i \geq 2$ and $i \geq 3$ respectively,

Note that, for both the $pp \to t\bar{t}W^{\pm}$ and $pp \to t\bar{t}t\bar{t}$ processes, we do not include the (finite) contributions from the real-emission of heavy particles ($W^{\pm}$, Z and H bosons and top quarks), sometimes called the "heavy-boson-radiation (HBR) contributions". Although they can be formally considered as part of the inclusive predictions at complete-NLO accuracy, these finite contributions are typically small and generally lead to very different collider signatures.[3]

Eqs. (2.5) and (2.6) define the NLO corrections in an additive approach. Another possibility would be applying the corrections multiplicatively, which is not uncommon

[2] As discussed in ref. [17], this classification of terms entering at a given order is not well defined; some diagrams can be viewed both as a "QCD correction" and an "EW correction" to different tree-level diagrams. Nevertheless, this intuitive classification is useful for understanding the underlying structure of such calculations. For this reason we use these expressions within quotation marks.

[3] HBR contributions to NLO_2 in $t\bar{t}W^{\pm}$ production have been provided in ref. [18].

JHEP02(2018)031

when combining NLO QCD and NLO EW corrections. The difference between the two approaches only enters at the NNLO-level and is formally beyond the accuracy of our calculations. The typical example where the multiplicative approach is well-motivated is when the NLO_1 corrections are dominated by soft-QCD physics, and the NLO_2 corrections by large EW Sudakov logarithms. Since these two corrections almost completely factorise, it can be expected that the mixed NNLO $\mathcal{O}(\alpha_s\alpha)$ corrections to LO_1 are dominated by the product of the $\mathcal{O}(\alpha_s)$ and $\mathcal{O}(\alpha)$ corrections, i.e., the NLO_1 and NLO_2 contributions. Hence, in this case, the dominant contribution to the mixed NNLO corrections can be taken into account by simply combining NLO corrections in the multiplicative approach. However, for $t\bar{t}W^{\pm}$ production, the NLO_1 terms are dominated by hard radiation, as we argued above. Therefore, even though the NLO_2 is dominated by large Sudakov logarithms, the multiplicative approach leads to uncontrolled NNLO terms. Moreover, due to the opening of the $tW \to tW$ scattering, the same would apply also for a multiplicative combination with the NLO_3. A similar argument is present for $t\bar{t}t\bar{t}$ production: for $i \leq 3$, the NLO_i terms are dominated by "QCD corrections" on top of the LO_i terms. Since the various LO_i have clearly different underlying structures due to the possibility of EW $tt \to tt$ scattering, also in this case there is no reason for believing that their NLO corrections factorise at NNLO and therefore that mixed NNLO corrections are dominated by products of NLO_i corrections. Hence, for both the $pp \to t\bar{t}W^{\pm}$ and $pp \to t\bar{t}t\bar{t}$ processes, not only the multiplicative approach is not leading to improved predictions, but there are clear indications to the fact that this approximation introduces uncontrolled terms. Thus, we use only the additive one.

Before discussing the numerical results of the complete-NLO predictions in the next section, we would like to mention that the calculation for $t\bar{t}t\bar{t}$ production shows a remarkably rich structure for the NLO_3 and NLO_4 contributions. As already said, the $q\bar{q} \to t\bar{t}t\bar{t}$ Born amplitude contains $\mathcal{O}(\alpha_s^2)$, $\mathcal{O}(\alpha_s\alpha)$ and $\mathcal{O}(\alpha^2)$ diagrams, and for this reason, the $q\bar{q} \to t\bar{t}t\bar{t}$ process contributes to LO_3 via both the square of its $\mathcal{O}(\alpha_s\alpha)$ Born amplitude and the interference of its $\mathcal{O}(\alpha_s^2)$ and $\mathcal{O}(\alpha^2)$ Born amplitudes. In order to have such a double structure at the leading order, it is necessary to have at least six external particles that are all coloured and EW interacting at the same time. Since each NLO_i is given by "QCD corrections" on top of the LO_i and by "EW corrections" on top of the LO_{i-1}, the NLO_3 and NLO_4 virtual corrections to $q\bar{q} \to t\bar{t}t\bar{t}$ extend this double structure to *three* different interference (or squared) terms: two originating from LO_3 and one from either LO_2 (in the case of NLO_3) or LO_4 (in the case of NLO_4). This is the first time that a calculation with such a triple structure for the virtual corrections has been performed.

3 Numerical results

In this section, we present numerical results for the complete-NLO predictions for the $t\bar{t}W^{\pm}$ and $t\bar{t}t\bar{t}$ production processes. As mentioned in the introduction, we used an extension of the MadGraph5_aMC@NLO framework for all our numerical studies. This extension has already been used for the calculation of complete-NLO corrections as already mentioned in the introduction. In MadGraph5_aMC@NLO, infra-red singularities are dealt with via the FKS method [44, 45] (automated in the module MadFKS [46, 47]). One-loop amplitudes

JHEP02(2018)031

are computed by dynamically switching between different kinds of techniques for integral reduction: the OPP [48], Laurent-series expansion [49], and tensor integral reduction [50–52]. These techniques have been automated in the module MadLoop [10], which is used for the generation of the amplitudes and in turn exploits CutTools [53], Ninja [54, 55] and Collier [56], together with an in-house implementation of the OpenLoops optimisation [5].

3.1 Input parameters

In the following we specify the common set of input parameters that are used in the $pp \to t\bar{t}W^{\pm}$ and $pp \to t\bar{t}t\bar{t}$ calculations. The masses of the heavy SM particles are set to

$$m_t = 173.34 \text{ GeV}\,, \quad m_H = 125 \text{ GeV}\,, \quad m_W = 80.385 \text{ GeV}\,, \quad m_Z = 91.1876 \text{ GeV}\,, \tag{3.1}$$

while all the other masses are set equal to zero. We employ the on-shell renormalisation for all the masses and set all the decay widths equal to zero. The renormalisation of α_s is performed in the $\overline{\text{MS}}$-scheme with five active flavours,[4] while the EW input parameters and the associated condition for the renormalisation of α are in the G_μ-scheme, with

$$G_\mu = 1.16639 \cdot 10^{-5} \text{ GeV}^{-2}\,. \tag{3.2}$$

The CKM matrix is set equal to the 3×3 unity matrix.

We employ dynamical definitions for the renormalisation (μ_r) and factorisation (μ_f) scales. In particular, their common central value μ_c is defined as

$$\mu_c = \frac{H_T}{2} \quad \text{for} \quad t\bar{t}W^{\pm}\,, \tag{3.3}$$

$$\mu_c = \frac{H_T}{4} \quad \text{for} \quad t\bar{t}t\bar{t}\,, \tag{3.4}$$

where

$$H_T \equiv \sum_{i=1,N(+1)} m_{T,i}\,, \tag{3.5}$$

and $m_{T,i} \equiv \sqrt{m_i^2 + p_T^2(i)}$ are the transverse masses of the $N(+1)$ final-state particles. Our scale choice for $t\bar{t}t\bar{t}$ production is motivated by the study in ref. [38]. Theoretical uncertainties due to the scale definition are estimated via the independent variation of μ_r and μ_f in the interval $\{\mu_c/2, 2\mu_c\}$. In order to show the scale dependence of $(\text{N})\text{LO}_i/\text{LO}_{\text{QCD}}$ relative corrections we will also consider the diagonal variation $\mu_r = \mu_f$, simultaneously in the numerator and the denominator. This scale dependence does not directly indicate scale uncertainties, but it will be very useful in our discussion.

Concerning the PDFs, we use the `LUXqed_plus_PDF4LHC15_nnlo_100` set [57, 58], which is in turn based on the PDF4LHC set [59–62]. This PDF set includes NLO QED effects in the DGLAP evolution and especially the most precise determination of the photon density.

[4] With the unit CKM matrix no b quarks are present in the initial state for $t\bar{t}W^{\pm}$ production, while for $t\bar{t}t\bar{t}$ their relative effect w.r.t. LO_1 is at or below the per-mil level.

JHEP02(2018)031

σ[fb]	LO_{QCD}	$\text{LO}_{\text{QCD}} + \text{NLO}_{\text{QCD}}$	LO	LO + NLO	$\frac{\text{LO+NLO}}{\text{LO}_{\text{QCD}}+\text{NLO}_{\text{QCD}}}$
$\mu = H_T/2$	$363^{+24\%}_{-18\%}$	$544^{+11\%}_{-11\%}\,(456^{+5\%}_{-7\%})$	$366^{+23\%}_{-18\%}$	$577^{+11\%}_{-11\%}\,(476^{+5\%}_{-7\%})$	1.06 (1.04)

Table 1. Cross sections for $t\bar{t}W^{\pm}$ production at 13 TeV in various approximations. The numbers in parentheses are obtained with the jet veto of eq. (3.6) applied.

σ[pb]	LO_{QCD}	$\text{LO}_{\text{QCD}} + \text{NLO}_{\text{QCD}}$	LO	LO + NLO	$\frac{\text{LO+NLO}}{\text{LO}_{\text{QCD}}+\text{NLO}_{\text{QCD}}}$
$\mu = H_T/2$	$6.64^{+28\%}_{-21\%}$	$16.58^{+17\%}_{-15\%}\,(11.37^{+11\%}_{-12\%})$	$6.72^{+27\%}_{-21\%}$	$20.86^{+15\%}_{-14\%}\,(14.80^{+11\%}_{-11\%})$	1.26 (1.30)

Table 2. Same as in table 1 but for 100 TeV.

3.2 Results for $pp \to t\bar{t}W^{\pm}$ production

We start by presenting predictions for $pp \to t\bar{t}W^{\pm}$ total cross sections at 13 and 100 TeV proton-proton collisions with and without applying a jet veto and then we discuss results at the differential level. The total cross sections at 13 TeV for $t\bar{t}W^{\pm}$ production are shown in table 1 at different accuracies, namely, LO_{QCD}, $\text{LO}_{\text{QCD}} + \text{NLO}_{\text{QCD}}$, LO and LO + NLO. We also show for each value its relative scale uncertainty and we provide the ratio of the predictions at LO + NLO and $\text{LO}_{\text{QCD}} + \text{NLO}_{\text{QCD}}$ accuracy. Analogous results at 100 TeV are displayed in table 2. Numbers in parentheses refer to the case in which we apply a jet veto, rejecting all the events with

$$p_T(j) > 100 \text{ GeV} \quad \text{and} \quad |y(j)| < 2.5\,, \tag{3.6}$$

where also hard photons are considered as a jet.[5] The purpose of this jet veto will become clear in the discussion below. Further details about the size of the individual $(\text{N})\text{LO}_i$ terms are provide in table 3 (13 TeV) and table 4 (100 TeV), where we show predictions for the quantities

$$\delta_{(\text{N})\text{LO}_i}(\mu) = \frac{\Sigma_{(\text{N})\text{LO}_i}(\mu)}{\Sigma_{\text{LO}_{\text{QCD}}}(\mu)}\,, \tag{3.7}$$

where $\Sigma(\mu)$ is simply the total cross section evaluated at the scale $\mu_f = \mu_r = \mu$. In tables 3 and 4 we do not show the result for $\text{LO}_1 \equiv \text{LO}_{\text{QCD}}$, since it is by definition always equal to one, regardless of the value of μ. We want to stress that results in tables 3 and 4 do not show directly scale uncertainties; the value of μ is varied simultaneously in the numerator and the denominator of δ. The purpose of studying δ as a function of μ will become clear below when we discuss the different dependence in δ_{NLO_1} versus δ_{NLO_2} and δ_{NLO_3}.

From tables 1 and 2 it can be seen that the LO_{QCD} predictions, both at 13 and 100 TeV, have a scale dependence that is larger than 20%. Including the LO_i contributions with $i > 1$ changes the cross section by about 1% and leaves also the scale dependence almost unchanged. As discussed in section 2, the LO_2 is exactly zero due to colour, thus this small correction is entirely coming from the LO_3 contribution. In tables 3 and 4 it can be seen that

[5] We explicitly verified that vetoing only quark and gluons, but not photons, leads to differences below the percent level. Moreover, from an experimental point of view, vetoing jets that are not isolated photons would be simply an additional complication.

JHEP02(2018)031

δ[%]	$\mu = H_T/4$	$\mu = H_T/2$	$\mu = H_T$
LO_2	-	-	-
LO_3	0.8	0.9	1.1
NLO_1	34.8 (7.0)	50.0 (25.7)	63.4 (42.0)
NLO_2	−4.4 (−4.8)	−4.2 (−4.6)	−4.0 (−4.4)
NLO_3	11.9 (8.9)	12.2 (9.1)	12.5 (9.3)
NLO_4	0.02 (−0.02)	0.04 (−0.02)	0.05 (−0.01)

Table 3. $\sigma_{(\text{N})\text{LO}_i}/\sigma_{\text{LO}_{\text{QCD}}}$ ratios for $t\bar{t}W^{\pm}$ production at 13 TeV for various values of $\mu = \mu_r = \mu_f$.

the scale dependence of this LO_3 contribution is slightly different from the LO_1. The factorisation scale dependence is almost identical for the LO_1 and LO_3 terms (both are $q\bar{q}'$ initiated and have similar kinematic dependence), thus this difference is entirely due to the variation of the renormalisation scale, which, at leading order, only enters the running of α_s. The LO_1 has two powers of α_s while the LO_3 has none. The value of α_s decreases with increasing scales, and therefore, it is no surprise that δ_{LO_3} increases with larger values for the scales.

As already known, in $t\bar{t}W^{\pm}$ production NLO QCD corrections are large and lead to a reduction of the scale uncertainty. Indeed, for the central scale choice, the total cross section at 13 TeV increases by 50% when including the NLO_{QCD} contribution, and a massive 150% correction is present at 100 TeV. The reduction in the scale dependence is about a factor two for 13 TeV, resulting in an 11% uncertainty. On the other hand, given the large NLO_{QCD} corrections, at 100 TeV the resulting scale dependence at $\text{LO}_{\text{QCD}} + \text{NLO}_{\text{QCD}}$ is larger than at 13 TeV, remaining at about 16%. Comparing these pure-QCD predictions to the complete-NLO cross sections (LO + NLO) we see that the latter are about 6% larger at 13 TeV, while the relative scale dependencies are identical. At 100 TeV, even though the relative scale dependence at complete-NLO is 1-2 percentage points smaller than at $\text{LO}_{\text{QCD}} + \text{NLO}_{\text{QCD}}$, in absolute terms it is actually larger. This effect is due to the large increase of about 26% induced by $(\text{N})\text{LO}_i$ terms with $i > 1$. Indeed, this increase is mostly coming from the contribution of the $tW \to tW$ scattering, which appears at NLO_3 via the quark real-emission and has a Born-like scale dependence. However, this dependence is relatively small since the NLO_3 involves only a single power of α_s.

In tables 3 and 4 we can see that $\delta_{\text{NLO}_1} \equiv \delta_{\text{NLO}_{\text{QCD}}}$ is strongly μ dependent, while this is not the case for δ_{NLO_i} with $i > 1$. In fact, this behaviour is quite generic and not restricted to $t\bar{t}W^{\pm}$ production; it can be observed for a wide class of processes. The μ dependence in δ_{NLO_1} leads to the reduction of the scale dependence of $\text{LO}_{\text{QCD}} + \text{NLO}_{\text{QCD}}$ results w.r.t. the LO_{QCD} ones. On the contrary, the δ_{NLO_i} quantities with $i > 1$ are typically quite independent of the value of μ. The reason is the following. The NLO_i contributions are given by "QCD corrections" to LO_i contributions as well "EW corrections" to the LO_{i-1} ones. The former involve explicit logarithms of μ due the renormalisation of both α_s and PDFs, while the latter contain only explicit logarithms of μ due the $\mathcal{O}(\alpha)$ PDFs counterterms. Indeed, in the G_μ-scheme, or other schemes such as $\alpha(0)$ or $\alpha(m_Z)$, the numerical input for α does

JHEP02(2018)031

δ[%]	$\mu = H_T/4$	$\mu = H_T/2$	$\mu = H_T$
LO_2	-	-	-
LO_3	0.9	1.1	1.3
NLO_1	159.5 (69.8)	149.5 (71.1)	142.7 (73.4)
NLO_2	−5.8 (−6.4)	−5.6 (−6.2)	−5.4 (−6.1)
NLO_3	67.5 (55.6)	68.8 (56.6)	70.0 (57.6)
NLO_4	0.2 (0.1)	0.2 (0.2)	0.3 (0.2)

Table 4. $\sigma_{(\text{N})\text{LO}_i}/\sigma_{\text{LO}_{\text{QCD}}}$ ratios for $t\bar{t}W^{\pm}$ production at 100 TeV for various values of $\mu = \mu_r = \mu_f$.

not depend on an external renormalisation scale. Moreover, the $\mathcal{O}(\alpha)$ PDF counterterms induce a much smaller effect than those of QCD, since they are $\mathcal{O}(\alpha/\alpha_s)$ suppressed and do not directly involve the gluon PDF. Thus, for a generic process, since a LO_i contribution is typically quite suppressed w.r.t. the LO_{i-1} one — or even absent, as e.g. for (multi) EW vector boson production — the scale dependence of δ_{NLO_i} with $i > 1$ is small. For this reason it is customary, and typically also reasonable, to quote NLO EW corrections independently from the scale definition. As can be seen in tables 3 and 4 this is also correct for $t\bar{t}W^{\pm}$, but as we will see in the next section the situation is quite different for $t\bar{t}t\bar{t}$ production, where also the $\delta_{(\text{N})\text{LO}_i}(\mu)$ quantities with $i > 1$ strongly depend on the value of μ.

By considering the μ dependence of the $\delta_{\text{NLO}_1}(\mu)$ contributions in tables 3 and 4, we see a different behaviour in the two tables. At 13 TeV the scale dependence of $\delta_{\text{NLO}_{\text{QCD}}}(\mu)$ increases with increasing scales. This is to be expected: the LO_1 contribution has a large renormalisation-scale dependence, resulting in a rapidly decreasing cross section with increasing scales. In order to counterbalance this, the scale dependence of the NLO_1 contribution must be opposite so that the scale dependence at NLO QCD accuracy is reduced. On the other hand, at 100 TeV, the scale dependence of the $\delta_{\text{NLO}_1}(\mu)$ decreases with increasing scales, suggesting that the scale dependence at $\text{LO}_{\text{QCD}} + \text{NLO}_{\text{QCD}}$ is actually larger than at LO_{QCD}. As can be seen in table 2 this does not appear to be the case. The reason is that contrary to 13 TeV, at 100 TeV collision energy the LO_{QCD} has not only a large renormalisation-scale dependence, but also the factorisation-scale one is sizeable. In fact, the scale dependence in table 2 is dominated by terms in which μ_r and μ_f are varied in opposite directions, i.e., $\{\mu_r, \mu_f\} = \{2\mu_c, \mu_c/2\}$ and $\{2\mu_c, \mu_c/2\}$. However, in table 4 we only consider the simultaneous variation of μ_r and μ_f. If we had estimated the scale uncertainty in tables 1 and 2 by only varying $\mu = \mu_r = \mu_f$, we would actually have seen an increment of the uncertainties in moving from LO_{QCD} to $\text{LO}_{\text{QCD}} + \text{NLO}_{\text{QCD}}$.

The NLO EW corrections, the NLO_2 contribution, are negative and have a −4-6% impact w.r.t. the LO_1 cross section. This is well within the $\text{LO}_{\text{QCD}}+\text{NLO}_{\text{QCD}}$ scale uncertainties. The opening of the $tW \to tW$ scattering enhances the NLO_3 contribution enormously. In fact, it is much larger than the NLO_2 terms, yielding a +12% effect at 13 TeV and almost a +70% increase of the cross section at 100 TeV, both w.r.t. LO_{QCD}. While at 13 TeV this is still within the $\text{LO}_{\text{QCD}} + \text{NLO}_{\text{QCD}}$ scale uncertainty band, this is not at all the case at

JHEP02(2018)031

100 TeV. Indeed, it is these NLO_3 contributions that are responsible for the enhancement in the cross sections at the complete-NLO level as compared to the $\text{LO}_{\text{QCD}} + \text{NLO}_{\text{QCD}}$ ones, as presented in the last column of tables 1 and 2. Hence, they must be included for accurate predictions for $pp \to t\bar{t}W^{\pm}$ cross sections. Conversely, the NLO_4 contributions are at the sub-percent level and can be neglected in all phenomenologically relevant studies.

Applying a jet veto, such as the one of eq. (3.6), impacts only the real-emission corrections for $t\bar{t}W^{\pm}$ production. All the LO_i terms remain unaffected and, since the dominant NLO real-emission contributions for this process are positive, the NLO_i cross sections decrease. This is also what one expects from a physical point of view: the jet veto cuts away part of the available phase space, resulting in a decrease in the number of expected events. Indeed, in tables 3 and 4 we can see that this is the case (for all values of μ). On the other hand, not all the NLO_i are affected in the same way by the jet veto. The NLO_{QCD} contribution is reduced by a large amount, about a factor two for the central value of the scales, while the reduction in the other NLO_i cross sections is much smaller. The reason for this difference is the following: a large fraction of the NLO_1 contribution originates from hard radiation, mainly due to the opening of the quark-gluon luminosity and the double logarithmic enhancement due to the radiation of a relatively soft/collinear W boson from a hard quark jet, cf., the left diagram of figure 2. Instead, the $\text{NLO}_2 \equiv \text{NLO}_{\text{EW}}$ is dominated by "EW corrections" to LO_1 and, therefore, does not involve a large increase due to the opening of the qg initiated real-emission contributions. Hence, the effect from the jet veto is strongly reduced. On the other hand, the NLO_3 does contain the enhancement from the gluon luminosity and is completely dominated by the $tW \to tW$ scattering, which is part of the real-emission contributions, see the right diagram of figure 2 and the discussion in section 2. Even so, these contributions are not very strongly affected by the jet veto, since the jet in $tW \to tW$ scattering is going mostly in the forward directions, which are unaffected by the central jet veto of eq. (3.6). The jet veto may be customised in order to enhance or suppress the NLO_i contributions, e.g., to study the impact of $tW \to tW$ scattering in more detail. However, it should be noted that a stronger jet veto would further suppress the NLO_i contributions, but it may also lead to unreliable results at fixed-order, due to the presence of unresummed large and negative contributions from QCD Sudakov logarithms. We leave a detailed study of the effects of various jet vetoes for future work.

On the total cross sections, see tables 1 and 2, the effect of the jet veto is not only manifest in the reduction of the $\text{LO}_{\text{QCD}} + \text{NLO}_{\text{QCD}}$ and $\text{LO} + \text{NLO}$ cross sections, but also in their greatly-reduced scale uncertainties. The latter are almost halved for the 13 TeV cross sections and reduced to about 11% at 100 TeV. This is another confirmation that the NLO_{QCD} is dominated by hard radiation due to the opening of additional production channels, which have a large tree-level induced scale dependence. This reduction of the uncertainties coming from scale variations means that the difference between the purely QCD calculation and complete-NLO predictions becomes of the same order as the scale uncertainties (at 13 TeV) or even considerably larger (at 100 TeV). Hence, with the jet veto applied, it becomes even more important to include the NLO_3 contribution for a reliable prediction of the cross section for $t\bar{t}W^{\pm}$ hadroproduction. We stress that the inclusion of only NLO EW corrections leads to a smaller shift and in the opposite direction.

JHEP02(2018)031

Differential distributions. Results for three representative distributions, $m(t\bar{t})$, $p_T(W^{\pm})$ and $p_T(t\bar{t})$, are shown for 13 TeV in figure 5 and for 100 TeV in figure 6. We consider the observables without (the plots on the left) and with (the plots on the right) the jet veto of eq. (3.6). Each plot has the following layout. The main panel shows distributions at NLO QCD (black) and complete-NLO (pink) accuracy, including scale variation uncertainties. For reference, we include also the LO_{QCD} central value ($\mu = \mu_c \equiv H_T/2$) as a black-dashed line.[6] The lower insets show three different quantities, all normalised to the central value of the $\text{LO}_{\text{QCD}} + \text{NLO}_{\text{QCD}}$ prediction. The grey band is the $\text{LO}_{\text{QCD}} + \text{NLO}_{\text{QCD}}$ prediction including scale-uncertainties and the pink band is the one at complete-NLO accuracy, i.e., they are the same quantities in the main panel but normalised. The blue band is instead what is typically denoted as the result at "NLO QCD + EW" accuracy, namely, the $\text{LO}_{\text{QCD}} + \text{NLO}_{\text{QCD}} + \text{NLO}_{\text{EW}}$ prediction. Via the comparison of these three quantities one can see at the same time the difference between results at NLO QCD and complete-NLO accuracy but also their differences with NLO QCD + EW results, which have already been presented in refs. [18].

At 13 TeV and without the jet veto (left plots of figure 5), the predictions for the three observables at the various levels of accuracy presented, coincide within their respective scale uncertainties. For the $m(t\bar{t})$ and, in particular the $p_T(W^{\pm})$, we see that the NLO EW corrections are negative and increase (in absolute value) towards the tails of the two distributions as expected from EW Sudakov logarithms coming from the virtual corrections. Only in the very tail of the distributions, close to $m(t\bar{t}) \sim 2000$ GeV and $p_T(W^{\pm}) \sim 2000$ GeV the uncertainty bands of the NLO QCD and NLO QCD + EW predictions no longer overlap. As expected from the inclusive results, the complete-NLO results increase the NLO QCD + EW predictions such that they move again closer to the NLO QCD central value. Indeed, the NLO QCD and the complete-NLO bands do overlap for the complete phase-space range plotted. Moreover, the difference between the NLO QCD + EW predictions and the complete-NLO is close to a constant for these two observables. Conversely, applying the jet veto changes the picture. First, it is quite apparent that the relative impact of the NLO EW corrections is increased significantly, reaching up to -40% in the tail of the $p_T(W^{\pm})$ distribution, as compared to only -20% without the jet veto. The reason is obvious: the jet veto reduces the large contribution from the NLO_{QCD}, hence, relatively speaking the NLO_{EW} becomes more important. In other words, while the NLO_{QCD} has a large contribution from the real-emission corrections, and are therefore greatly affected by the jet veto, in this region of phase space the NLO_{EW} is dominated by the EW Sudakov logarithms, which are not influenced by the jet veto. The other important effect coming from the jet veto is the reduction of the scale uncertainties: as we have already seen at the inclusive level, this reduction is about a factor two for 13 TeV. For the $m(t\bar{t})$ and $p_T(W^{\pm})$ this also appears to be the case over the complete kinematic ranges plotted for the NLO QCD predictions. At small and intermediate ranges, this is also the case for the NLO QCD + EW and the complete-NLO results. On the other hand,

[6] Comparisons among the scale uncertainties of the LO_{QCD} and $\text{LO}_{\text{QCD}} + \text{NLO}_{\text{QCD}}$ result have been documented in detail for 13 and 100 TeV in refs. [38] and [63], respectively.

JHEP02(2018)031

in the far tails, the uncertainty bands from the NLO QCD + EW and, to a slightly lesser extend, the complete-NLO are increased. Again, this is no surprise, since, as we have just concluded, these predictions contain a large contribution from EW Sudakov corrections in the NLO_{EW}, which have the same large scale uncertainty as the LO_1. Given that, relatively speaking, these NLO_{EW} contributions become significantly more important with the jet veto, also the scale uncertainties become significantly larger.

For the third observable, $p_T(t\bar{t})$, the situation is extreme. This is mainly due to the fact that the NLO_{QCD} corrections are not constant over the phase space as was the case for $m(t\bar{t})$ and $p_T(W^{\pm})$. Rather, due to terms of order $\alpha_s \log^2(p_T^2(t\bar{t})/m_W^2)$ the NLO_{QCD} greatly enhances the LO_{QCD} predictions for moderate, and, in particular, large $p_T(t\bar{t})$. This enhancement originates from the real-emission $t\bar{t}W^{\pm}q$ final-states, where a soft and collinear $W^{\pm}$ can be emitted from the final-state quark (see left diagram in figure 2). Thus, while at the Born level the $t\bar{t}$ pair is always recoiling against the $W^{\pm}$ boson, at NLO QCD accuracy, for large $p_T(t\bar{t})$ values, it mainly recoils against a jet that is emitting the $W^{\pm}$ boson. More details about this mechanism can be found in ref. [38]. For this reason, without a jet veto, at NLO QCD accuracy very large corrections and scale uncertainties are present for large $p_T(t\bar{t})$ values. Indeed, the dominant NLO_{QCD} contribution, the soft and collinear emission of a $W^{\pm}$ boson from a final-state quark, is very large and does not lead to a reduction of the scale dependence.[7] Moreover, since the NLO_{QCD} are by far the dominant contributions, the effects from $(\text{N})\text{LO}_i$, with $i > 1$ are completely negligible at large transverse momenta. Only for intermediate transverse momenta, $80\,\text{GeV} < p_T(t\bar{t}) < 400\,\text{GeV}$, we see a small effect in the comparison of NLO QCD and complete-NLO.

On the other hand, with a jet veto, the NLO_{QCD} contribution (and therefore also the scale uncertainties) is strongly reduced. Indeed, when the jet veto is applied, hard-jets and the corresponding logarithmic enhancements are not present, and the $t\bar{t}$ pair is mostly recoiling directly against the $W^{\pm}$ boson, making the predictions for $p_T(t\bar{t})$ and $p_T(W^{\pm})$ very similar. The only difference is in the comparison of the NLO QCD and the complete-NLO predictions. For the $p_T(W^{\pm})$ observable, this difference is basically a constant in the region $30\,\text{GeV} < p_T(W^{\pm}) < 400\,\text{GeV}$. On the other hand, for $p_T(t\bar{t})$ we see that the NLO_3 contribution is not a constant: there is a reduction at small transverse momenta. Indeed, one would expect from $tW \to tW$ scattering that the transverse momenta of the top pair is typically larger than in the $(\text{N})\text{LO}_1$, due to the t-channel enhancement (between the $t\bar{t}$ and the $W^{\pm}j$ pairs) at large transverse momenta. This is somewhat washed-out for the $p_T(W^{\pm})$ since it is the W boson together with the jet that receive this enhancement.

At 100 TeV, see figure 6, the differences between the various predictions are qualitatively different from 13 TeV. The reason is that the opening of the qg-induced contributions in NLO_1 and the $tW \to tW$ scattering contribution in NLO_3 are much more dramatic. The central value of the complete-NLO predictions is typically outside of the NLO QCD band even though the scale uncertainties are larger at 100 TeV than at 13 TeV. Moreover, with the jet veto, the bands generally do not even touch, apart from where they cross at large $p_T(W^{\pm})$ and $p_T(t\bar{t})$.

[7] The size of the NLO_{QCD} contribution is the difference between the dashed and the solid black line.

JHEP02(2018)031

Without a jet veto, on the basis of all the previous considerations, also NLO corrections on top of the $t\bar{t}W^{\pm}j$ final state may be relevant for $t\bar{t}W^{\pm}$ inclusive production. Indeed sizeable effects are expected from QCD and EW corrections on top of the dominant $\alpha_s \log^2(p_T^2(t\bar{t})/m_W^2)$ contribution and the large NLO_3 one, both arising from the qg initial state. The former would lead also to a reduction of the scale dependence in the tail of the $p_T(t\bar{t})$ distribution, which is dominated by the $t\bar{t}W^{\pm}j$ final state. However, these contributions are part of the NNLO corrections to the inclusive $t\bar{t}W^{\pm}$ production and therefore are not available and not included in our calculation. A possible way for estimating these effects is merging $t\bar{t}W^{\pm}$ and $t\bar{t}W^{\pm}j$ (and $t\bar{t}W^{\pm}\gamma$) final states at NLO accuracy. In the case of NLO QCD corrections a study in this direction has been suggested for $t\bar{t}W^{\pm}$ production in ref. [38]. For NLO_{EW} and subleading NLO_i corrections a fully-consistent technology is not yet available to perform this kind of study.

Further details about individual NLO_i contributions at the differential level are given in figure 7 (13 TeV) and figure 8 (100 TeV). In the plots we show all the $\delta_{\text{NLO}_i}(\mu)$ for $\mu = \mu_c \equiv H_T/2$ (solid line), $\mu = \mu_c/2$ (dashed line) and $\mu = 2\mu_c$ (dotted line). We show the same distributions (with and without veto) as in figures 5 and 6. We remark again that the $\delta_{\text{NLO}_i}(\mu)$ do not show directly scale uncertainties since the value of μ is varied both in the numerator and the denominator of δ. On the other hand, we can directly see that also at the differential level the relative sizes of both NLO_2 and NLO_3 w.r.t. the LO_{QCD} are almost insensitive to the value of the scale; the corresponding solid, dashed and dotted lines are almost indistinguishable. As expected, also at the differential level the impact of the NLO_4 is completely negligible for the whole range of the distributions considered.

As could already have been concluded by comparing the dashed and solid black lines in figures 5 and 6, the NLO QCD corrections are not at all a constant over phase space. The solid black lines in figures 7 and 8 make this very clear. In particular for the $p_T(t\bar{t})$ distributions without the jet veto (lower left plots), the $\text{NLO}_1 \equiv \text{NLO}_{\text{QCD}}$ contribution easily becomes as large as the $\text{LO}_1 \equiv \text{LO}_{\text{QCD}}$ and increases to more than an order of magnitude larger than LO_1 at large transverse momenta in 100 TeV collisions. But also for $p_T(W^{\pm})$ we see large NLO QCD corrections, in particular at 100 TeV. On the other hand, for $m(t\bar{t})$ the NLO QCD corrections are mostly flat, in particular at 13 TeV. With the jet veto (plots on the right) the situation changes quite dramatically. The NLO QCD corrections are, in general, under much better control, even though one can see that the extreme tails in the $p_T(W^{\pm})$ and $p_T(t\bar{t})$ at 100 TeV the NLO_{QCD} contributions decrease rapidly and are starting to be strongly influenced by logarithms related to the jet-veto scale. If one would look at even larger transverse momenta, or, equivalently, reduce the jet-veto scale, these logarithms will grow and eventually fixed-order perturbation theory would break down, showing the need for resummation of these jet-veto logarithms.

Since these plots are normalised w.r.t. the LO_1 (cf., the lower insets of figures 5 and 6 which are normalised to LO_1+NLO_1), one can clearly see the effects of the NLO EW corrections, i.e., the NLO_2, independently from the NLO QCD corrections. One sees the typical EW Sudakov logarithms: negligible effects at the percent level at small and moderate $t\bar{t}$ invariant masses and $W^{\pm}$ and $t\bar{t}$ transverse momenta, but growing rapidly with increasing values of the observables, to about -20% at $m(t\bar{t}) \simeq 2000$ GeV and -40% at $p_T(W^{\pm}) \simeq$

JHEP02(2018)031

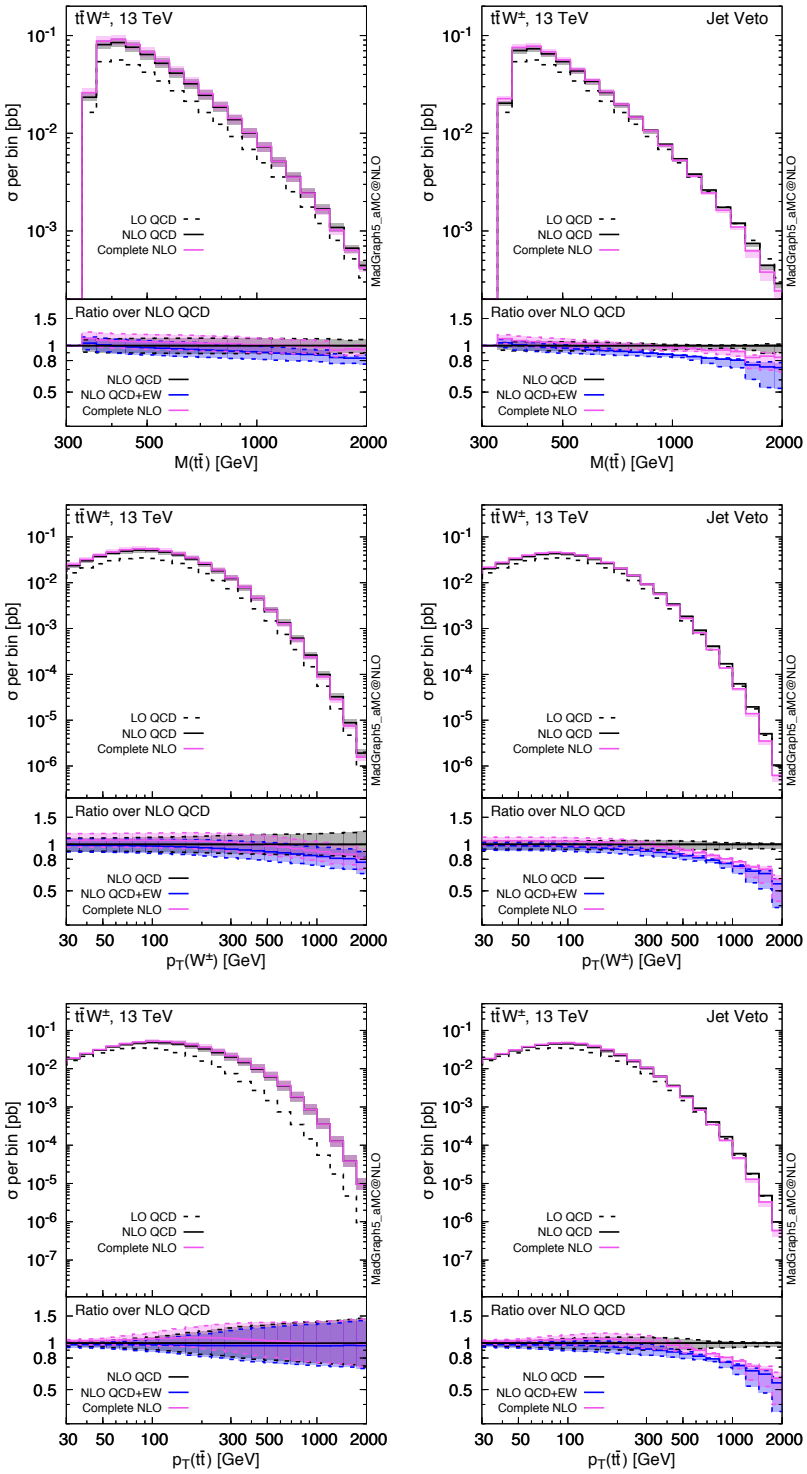

Figure 5. Differential distributions for $t\bar{t}W^{\pm}$ production at 13 TeV. For the plots on the right, the jet veto of eq. (3.6) has been applied. The main panels show the scale-uncertainty bands for $\mathrm{LO_{QCD}} + \mathrm{NLO_{QCD}}$ (black) and LO + NLO (pink), and central value of $\mathrm{LO_{QCD}}$; in the lower inset the scale-uncertainty bands are normalised to the $\mathrm{LO_{QCD}} + \mathrm{NLO_{QCD}}$ central value and also the $\mathrm{LO_{QCD}} + \mathrm{NLO_{QCD}} + \mathrm{NLO_{EW}}$ prediction (blue) is displayed.

JHEP02(2018)031

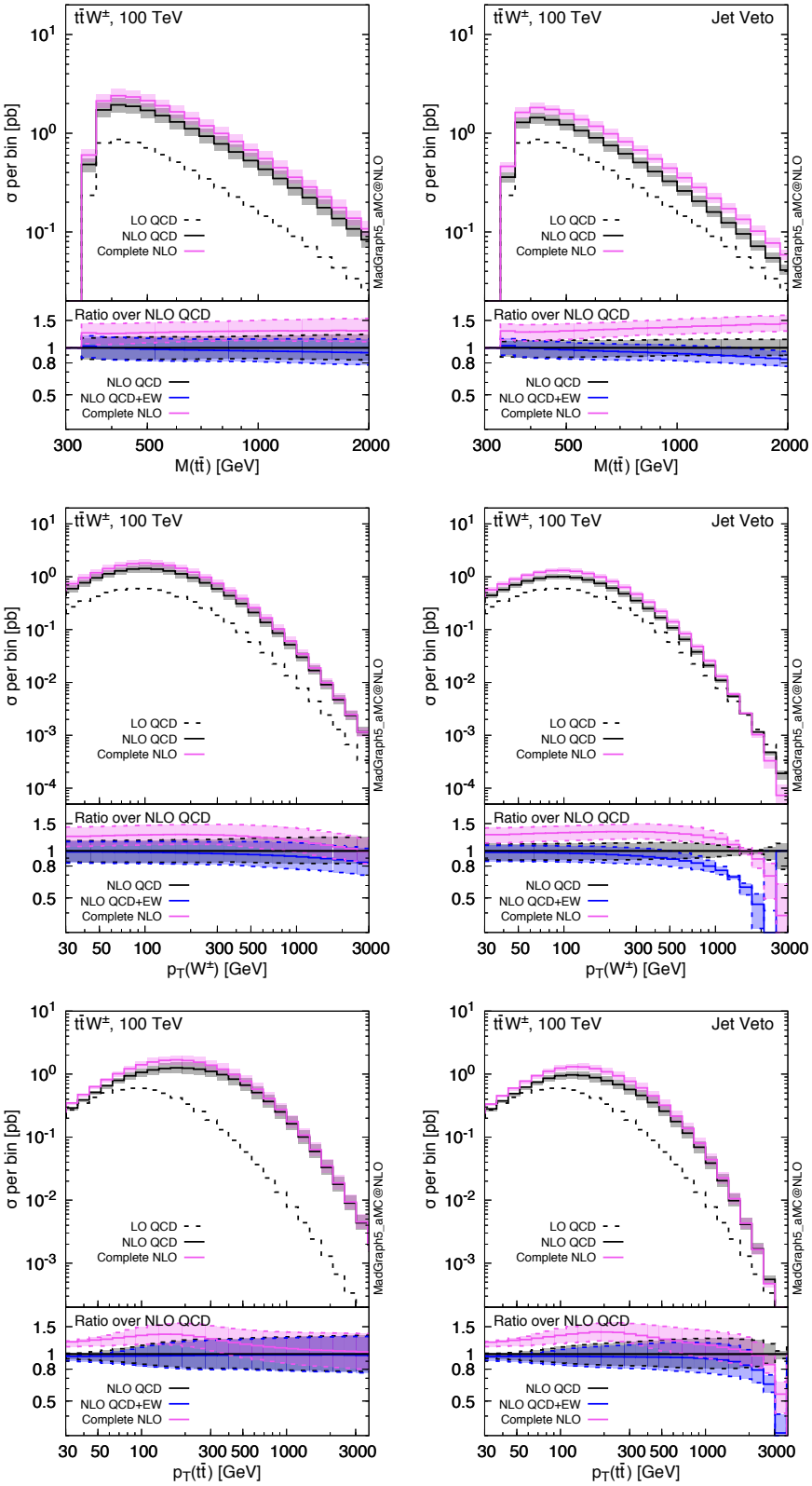

Figure 6. Same as figure 5 but for 100 TeV collisions.

JHEP02(2018)031

$p_T(t\bar{t}) \simeq 2000\,\text{GeV}$. The fact that the NLO EW corrections are smaller for $m(t\bar{t})$ in comparison to $p_T(W^\pm)$ and $p_T(t\bar{t})$ is no surprise since the impact of the EW Sudakov logarithms is related to the number of invariants that are large for the observable considered. Typically, for large invariant masses, there need to be fewer large invariants than for producing large transverse momenta. The size of the NLO EW corrections relative to the LO_1 is quite similar for 13 TeV and 100 TeV collisions. Moreover, by comparing the distributions with and without the jet veto we also see that their sizes are hardly influenced by the jet veto.

At variance with the NLO_2 term, at 13 TeV the NLO_3 contribution is much more constant w.r.t. the LO_1 over the whole phase space. Indeed, for the $m(t\bar{t})$ the δ_{NLO_3} is effectively a constant, increasing the LO_1 cross section by about 12% (which is reduced by applying the jet veto to about 9%). Similarly, for the $p_T(W^\pm)$ distribution, the NLO_3 correction is fairly flat. On the other hand, the $p_T(t\bar{t})$ does show some kinematic dependence in the δ_{NLO_3} ratio. It is small at small transverse momenta, increases at intermediate values and, in particular when the jet veto is applied, it decreases again at large values of $p_T(t\bar{t})$. This is consistent with what we found in the comparing the $\text{LO}_{\text{QCD}} + \text{NLO}_{\text{QCD}}$ and NLO QCD + EW predictions in figure 5. At 100 TeV the NLO_3 contributions are large and the δ_{NLO_3} plots are not at all flat in the phase space. As at 13 TeV, the effects are most dramatic in the $p_T(t\bar{t})$ distributions, which show a large hump at around 500 GeV (1 TeV) with (without) the jet veto. However, as discussed before, without a jet veto, at large $p_T(t\bar{t})$ the NLO_{QCD} corrections is giant and is even the dominant contribution among all the $(\text{N})\text{LO}_i$ ones, including the LO_1. For this reason, although δ_{NLO_2} and δ_{NLO_3} are large at high $p_T(t\bar{t})$, results at $\text{LO}_{\text{QCD}} + \text{NLO}_{\text{QCD}}$, $\text{LO}_{\text{QCD}} + \text{NLO}_{\text{QCD}} + \text{NLO}_{\text{EW}}$, and $\text{LO} + \text{NLO}$ accuracies are very close to each other; the three predictions are all dominated by NLO_{QCD}, while δ_{NLO_i} are normalised to LO_{QCD}.

The application of a jet veto as in eq. (3.6) may be exploited in BSM analyses such as the one described in ref. [33]; rather than requiring a forward jet it may be possible to observe enhancements in the $tW^\pm \to tW^\pm$ scattering directly in $t\bar{t}W^\pm$ production by vetoing hard central jets.

JHEP02(2018)031

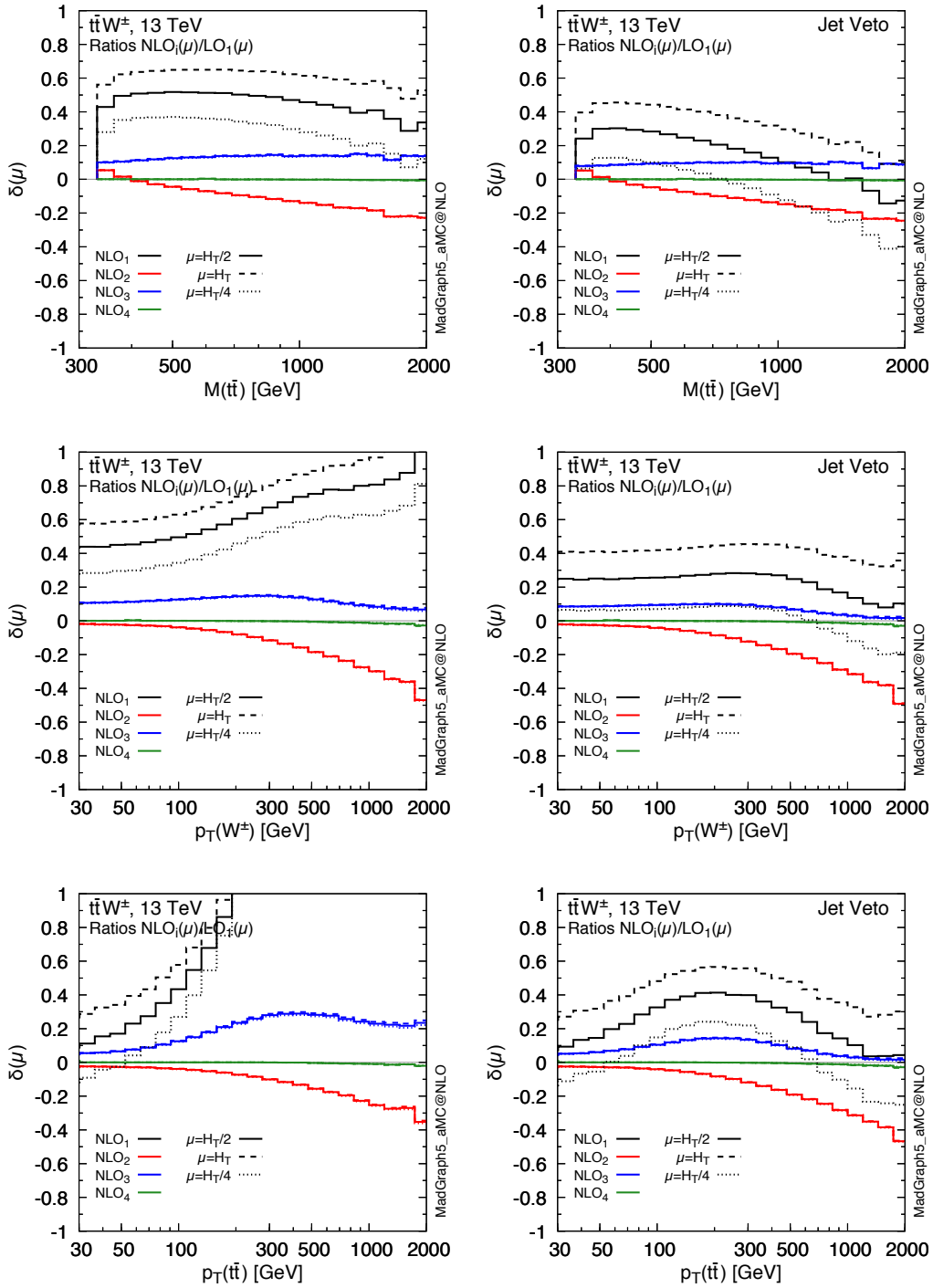

Figure 7. Individual NLO_i contributions to $t\bar{t}W^{\pm}$ production at 13 TeV normalised to $\mathrm{LO}_1 \equiv \mathrm{LO}_{\mathrm{QCD}}$, for different values of the scale μ for the same distributions as considered in figure 5. These plots do not directly show scale uncertainties. Note that $\mathrm{NLO}_1 \equiv \mathrm{NLO}_{\mathrm{QCD}}$ and $\mathrm{NLO}_2 \equiv \mathrm{NLO}_{\mathrm{EW}}$.

JHEP02(2018)031

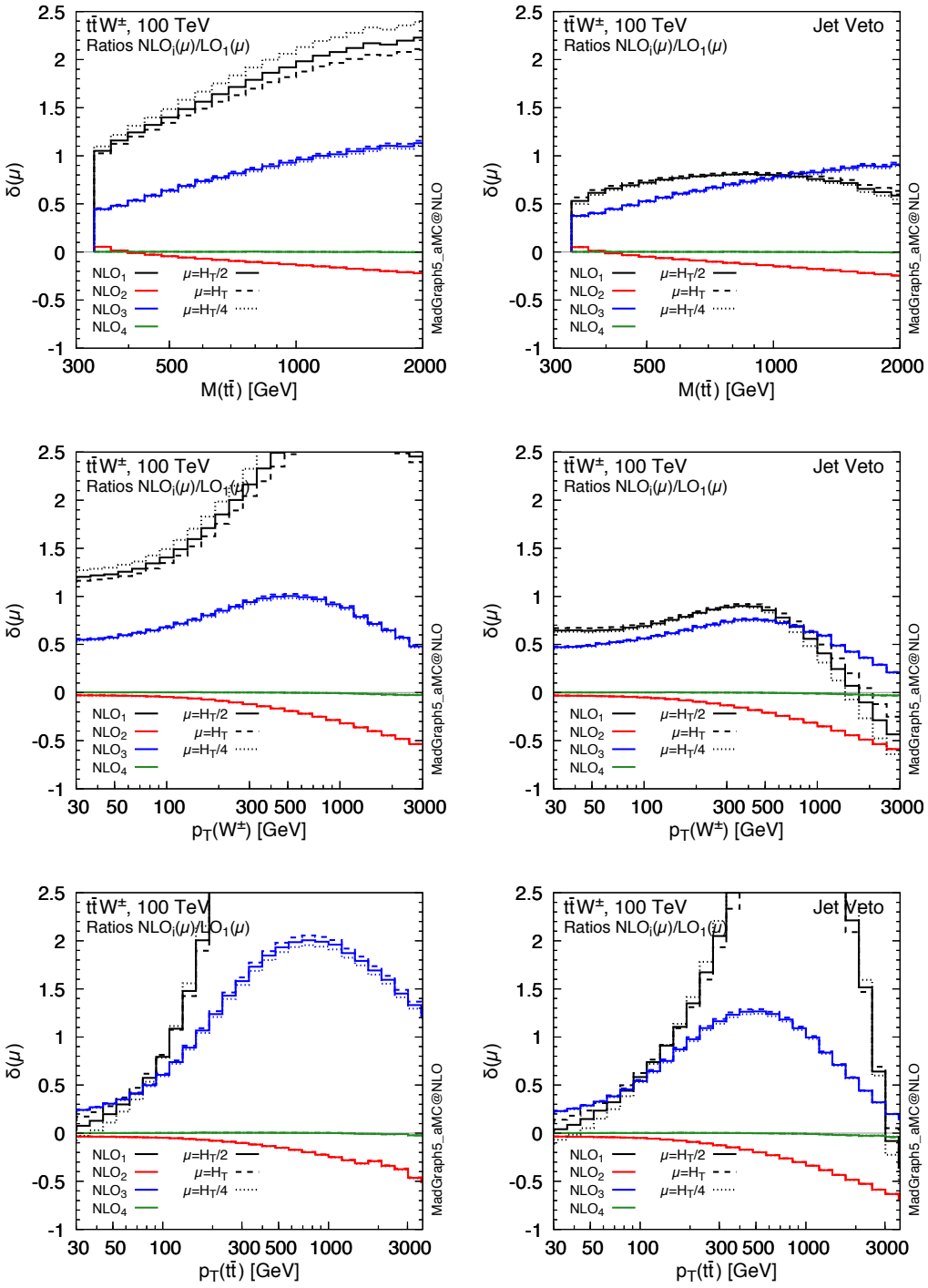

Figure 8. Same as figure 7 but for 100 TeV collisions.

JHEP02(2018)031

σ[fb]	LO_{QCD}	$\text{LO}_{\text{QCD}} + \text{NLO}_{\text{QCD}}$	LO	LO + NLO	$\frac{\text{LO(+NLO)}}{\text{LO}_{\text{QCD}}(+\text{NLO}_{\text{QCD}})}$
$\mu = H_T/4$	$6.83^{+70\%}_{-38\%}$	$11.12^{+19\%}_{-23\%}$	$7.59^{+64\%}_{-36\%}$	$11.97^{+18\%}_{-21\%}$	1.11 (1.08)

Table 5. Cross section for $pp \to t\bar{t}t\bar{t}$ at 13 TeV in various approximations.

σ[pb]	LO_{QCD}	$\text{LO}_{\text{QCD}} + \text{NLO}_{\text{QCD}}$	LO	LO + NLO	$\frac{\text{LO(+NLO)}}{\text{LO}_{\text{QCD}}(+\text{NLO}_{\text{QCD}})}$
$\mu = H_T/4$	$2.37^{+49\%}_{-31\%}$	$3.98^{+18\%}_{-19\%}$	$2.63^{+44\%}_{-28\%}$	$4.18^{+17\%}_{-17\%}$	1.11 (1.05)

Table 6. Same as in table 5 but for 100 TeV.

3.3 Results for $pp \to t\bar{t}t\bar{t}$ production

Similarly to the previous section, we start by presenting predictions for $t\bar{t}t\bar{t}$ total cross sections at 13 and 100 TeV proton-proton collisions and then we discuss results at the differential level. Using a layout that is similar to table 1, in table 5 we show 13 TeV predictions at LO_{QCD}, $\text{LO}_{\text{QCD}} + \text{NLO}_{\text{QCD}}$, LO and LO + NLO accuracies. We also display the $\text{LO}/\text{LO}_{\text{QCD}}$ and, in brackets, $(\text{LO} + \text{NLO})/(\text{LO}_{\text{QCD}} + \text{NLO}_{\text{QCD}})$ ratios. Results at 100 TeV are in table 6. In table 7, similarly to table 3, we show 13 TeV predictions for the $\delta_{(\text{N})\text{LO}_i}(\mu)$ ratios, and analogous results at 100 TeV are in table 8.

As can be seen in tables 5 and 6, the scale dependence is very large at LO_{QCD} and LO accuracy and it is strongly reduced both in the NLO QCD and complete-NLO predictions to about 20%. Nevertheless, it is still larger than the impact of the non-purely-QCD contributions, which is also reduced moving from LO to NLO accuracy, halved in the 100 TeV case. At the inclusive level, the difference between LO + NLO and LO_{QCD} + NLO_{QCD} predictions is well within their respective scale uncertainties, especially at 100 TeV where this difference is merely 5% of the $\text{LO}_{\text{QCD}} + \text{NLO}_{\text{QCD}}$ result. However, the numbers in tables 5 and 6 hide the most important feature of the complete-NLO result, i.e., very large and scale-dependent cancellations among the $(\text{N})\text{LO}_i$ terms with $i \geq 2$. This will become clear from the discussion in the next paragraph.

As anticipated in section 2, in $t\bar{t}t\bar{t}$ production the LO_2 and LO_3 contributions are not so suppressed w.r.t. the LO_{QCD}, at variance with $t\bar{t}W^{\pm}$ production (see tables 7 and 8, cf. tables 3 and 4). For $t\bar{t}t\bar{t}$ production, due to sizeable contributions from the EW $tt \to tt$ scattering, LO_2 and LO_3 can induce corrections of the order -30% and $+40\%$ on top of the LO_1, respectively.[8] Therefore, also the NLO_2 and NLO_3 contributions are large, since they contain "QCD corrections" to LO_2 and LO_3 terms, respectively. The fact that a large fraction of NLO_2 and NLO_3 contributions is of QCD origin can be understood by the μ-dependencies of δ_{NLO_2} and δ_{NLO_3} ratios, which, as can be seen in tables 7 and 8, are very large. Indeed, NLO_2 and NLO_3 terms involve explicit logarithms of μ that compensate the PDF and α_s scale dependence at LO_2 and LO_3 accuracy, respectively. Thus, in $t\bar{t}t\bar{t}$

[8] Similarly to the case of the LO_3 in $t\bar{t}W^{\pm}$ production, the scale dependences of the LO_2 and especially of the LO_3 are much smaller than that of LO_1, due to the different powers of α_s associated to them. Hence, with larger(smaller) values of the scales and consequently smaller(larger) values of LO_1, the δ_{LO_2} and δ_{LO_3} become larger(smaller) in absolute value.

JHEP02(2018)031

δ[%]	$\mu = H_T/8$	$\mu = H_T/4$	$\mu = H_T/2$
LO_2	-26.0	-28.3	-30.5
LO_3	32.6	39.0	45.9
LO_4	0.2	0.3	0.4
LO_5	0.02	0.03	0.05
NLO_1	14.0	62.7	103.5
NLO_2	8.6	-3.3	-15.1
NLO_3	-10.3	1.8	16.1
NLO_4	2.3	2.8	3.6
NLO_5	0.12	0.16	0.19
NLO_6	< 0.01	< 0.01	< 0.01
$\mathrm{NLO}_2 + \mathrm{NLO}_3$	-1.7	-1.6	0.9

Table 7. $t\bar{t}t\bar{t}$: $\sigma_{(\mathrm{N})\mathrm{LO}_i}/\sigma_{\mathrm{LO}_{\mathrm{QCD}}}$ ratios at 13 TeV, for different values of $\mu = \mu_r = \mu_f$.

production, at variance with most of the other production processes studied in the literature, quoting the relative size of $\mathrm{NLO}_{\mathrm{EW}} \equiv \mathrm{NLO}_2$ or NLO_3 corrections without specifying the QCD-renormalisation and factorisation scale is simply meaningless. Moreover, δ_{NLO_2} and δ_{NLO_3} corrections can *separately* be very large, easily reaching $\pm 15\%$ (depending on the value of μ). Surprisingly, for our central value of the renormalisation and factorisation scales, the δ_{NLO_2} and δ_{NLO_3} are almost zero,[9] particularly for 13 TeV. On the other hand, if we had taken $H_T/2$ or even $m_{t\bar{t}t\bar{t}}$ as our central scale choice, the NLO_2 and NLO_3 corrections relative to the LO_1, δ_{NLO_2} and δ_{NLO_3}, would have been much larger. Still, even for the central value $\mu = H_T/4$, the corrections are much larger than foreseen, especially for δ_{NLO_3} which naively is expected to be of order $\alpha_s^3\alpha^2/\alpha_s^4 = \alpha^2/\alpha_s \sim 0.1\%$ level. On the other hand, the relative cancellation observed between NLO_2 and NLO_3 contributions is even larger than in the case of LO_2 and LO_3. As can be seen in the last rows of tables 7 and 8, at the inclusive level the sum of the ratios $\delta_{\mathrm{NLO}_2} + \delta_{\mathrm{NLO}_3}$ is not only small, but also stable under scale variation,[10] resulting in corrections of at most a few percents w.r.t. the $\mathrm{LO}_{\mathrm{QCD}}$. Furthermore, particularly at 13 TeV, $\delta_{\mathrm{NLO}_2} + \delta_{\mathrm{NLO}_3}$ receives also additional cancellations when summed to δ_{NLO_4}, which itself is much larger than the expected $\alpha_s^2\alpha^3/\alpha_s^4 = \alpha^3/\alpha_s^2 \sim 0.01\%$ level. To the best of our understanding, these cancellations are accidental.

These large and accidental cancellations among the $(\mathrm{N})\mathrm{LO}_i$ terms with $i > 1$ are particularly relevant from a BSM perspective, since the level of these cancellations may be altered by new physics. As an example, we can refer to the case of an anomalous y_t coupling, which, as we have already mentioned, has been considered in the tree-level analysis of ref. [34]. Terms proportional to y_t^2 are present in all the $(\mathrm{N})\mathrm{LO}_i$ with $i \geq 2$ and terms

[9] Our choice for the central value of the scales has not been tuned in order to reduce the effects from the NLO_2 and NLO_3. Rather, it is motivated by the study in ref. [38], which deals only with the LO_1 and NLO_1.

[10] We verified this feature also with different functional forms for the scale μ.

JHEP02(2018)031

δ[%]	$\mu = H_T/8$	$\mu = H_T/4$	$\mu = H_T/2$
LO_2	-18.7	-20.7	-22.8
LO_3	26.3	31.8	37.8
LO_4	0.05	0.07	0.09
LO_5	0.03	0.05	0.08
NLO_1	33.9	68.2	98.0
NLO_2	-0.3	-5.7	-11.6
NLO_3	-3.9	1.7	8.9
NLO_4	0.7	0.9	1.2
NLO_5	0.12	0.14	0.16
NLO_6	< 0.01	< 0.01	< 0.01
$\text{NLO}_2 + \text{NLO}_3$	-4.2	-4.0	2.7

Table 8. $t\bar{t}t\bar{t}$: $\sigma_{(\text{N})\text{LO}_i}/\sigma_{\text{LO}_{\text{QCD}}}$ ratios at 100 TeV, for different values of $\mu = \mu_r = \mu_f$.

proportional to y_t^4 are present in all the (N)LO_i with $i \geq 3$, but also terms proportional to y_t^6 are present for any $i \geq 3$. Moreover, also contributions proportional to y_t, y_t^3 and y_t^5 are possible. Similar considerations apply also to other new physics effects in $t\bar{t}t\bar{t}$ production (see, e.g., ref. [64] and references therein for scenarios already analysed in the literature).

In order to understand the hierarchy of the different (N)LO_i contributions, it is important to note that at 13 TeV and especially at 100 TeV the total cross section is dominated by the gg initial state (see, e.g., ref. [38]). For this reason, the LO_4, LO_5, NLO_5 and NLO_6 contributions, which are vanishing for the gg initial state, are much smaller than the other contributions. The modest scale dependence of δ_{NLO_4} is also induced by this feature; the NLO_4 contribution mainly arises from "EW corrections" to gg-induced LO_3 contributions, which do not have any explicit dependence on μ; and therefore the scale dependence of the NLO_4 follows the scale dependence of the LO_3 to a large extent.

Differential distributions. We now move to the description of the results at the differential level, where we consider the following distributions: the invariant mass of the four (anti)top quarks $m(t\bar{t}t\bar{t})$ (figure 9), the sum of the transverse masses of all the particles in the final state H_T as defined in eq. (3.5) (figure 10), the transverse momenta of the hardest of the two top quarks $p_T(t_1)$ (figure 11), and the rapidity of the softest one $y(t_2)$ (figure 12). At variance with the case of $t\bar{t}W^{\pm}$ production in section 3.2, we organise plots according to the observable considered. In the figures we display 13 TeV results on the left and 100 TeV results on the right. In the upper plots of each of these figures we provide predictions at different levels of accuracy, using a similar layout[11] as in figures 5 and 6,

[11] At variance with $t\bar{t}W^{\pm}$ production, we do not show $\text{LO}_{\text{QCD}} + \text{NLO}_{\text{QCD}} + \text{NLO}_{\text{EW}}$ predictions. This level of accuracy is rather artificial, since the $\text{NLO}_{\text{EW}} \equiv \text{NLO}_2$ terms are dominated by "QCD corrections" to the LO_2 ones. Hence, including NLO_2 without LO_2 would not be very consistent. Moreover, there are large cancellations between LO_2 and LO_3, so, including only the former and not the latter would not be

JHEP02(2018)031

which is described in detail in section 3.2. Also for $t\bar{t}t\bar{t}$ production, comparisons among the scale uncertainties of the $\mathrm{LO_{QCD}}$ and $\mathrm{LO_{QCD}} + \mathrm{NLO_{QCD}}$ result have been documented in detail in ref. [38] for 13 TeV, so they are not repeated here. Individual contributions from the different $\mathrm{(N)LO}_i$ terms are instead displayed in the central and lower plots. In the central plots we show the $\delta_{\mathrm{(N)LO}_i}(\mu)$, see eq. (3.7), with $\mu = \mu_c \equiv H_T/4$, while the lower plots focus on $\mathrm{NLO_2}$ and $\mathrm{NLO_3}$ contributions and their sum featuring large cancellations. In particular, we show $\delta_{\mathrm{NLO_2}}(\mu)$, $\delta_{\mathrm{NLO_3}}(\mu)$ and their sum for $\mu = \mu_c$ (solid line), $\mu = \mu_c/2$ (dashed line) and $\mu = 2\mu_c$ (dotted line). In practice, the dark-blue and red solid lines are the same quantities in the middle and lower plots. Once again, we remark that the $\delta_{\mathrm{NLO}_i}(\mu)$ ratio does not show directly the scale uncertainty since the value of μ is varied both in the numerator and the denominator of δ.

Away from the threshold region, i.e., $m(t\bar{t}t\bar{t}) > 900\,\mathrm{GeV}$, the complete-NLO prediction for the four-top invariant-mass distribution is very close to the NLO QCD one, with an almost constant increase of about 10%, both at 13 and 100 TeV, see upper plots in figure 9. This increase is well within the uncertainty bands of either of the predictions. On the other hand, in the threshold region the enhancement of the cross section due to terms with $\mathrm{(N)LO}_i$, with $i > 1$, is much larger than for the inclusive results. In this region the central value of the complete-NLO predictions lies outside the $\mathrm{LO_1}+\mathrm{NLO_1}$ uncertainty band. From the central plots of figure 9, it can be seen that the $\mathrm{(N)LO_2}$ and $\mathrm{(N)LO_3}$ contributions are individually sizeable w.r.t. $\mathrm{LO_{QCD}}$ and their relative impact has a large dependence on kinematics, easily reaching several tens of percents in certain regions of phase space.

As anticipated from the inclusive results, there are large cancellations in the distributions among $\mathrm{LO_2}$ and $\mathrm{LO_3}$ contributions and especially among $\mathrm{NLO_2}$, $\mathrm{NLO_3}$ ones; the latter are explicitly shown in the lower plots. In particular, although the corresponding $\delta_{\mathrm{(N)LO}_i}$ terms individually depend on the value of $m(t\bar{t}t\bar{t})$, they lead for $m(t\bar{t}t\bar{t}) > 900\,\mathrm{GeV}$ to the aforementioned constant increase of about 10% of the complete-NLO prediction w.r.t. the NLO QCD result. As can be seen in the central plots, the $\delta_{\mathrm{LO_2}}$ is negative, it is about -10% at $m(t\bar{t}t\bar{t}) \simeq 4000\,\mathrm{GeV}$ and further decreases for smaller invariant masses, reaching about -40% at $m(t\bar{t}t\bar{t}) \simeq 900\,\mathrm{GeV}$. On the other hand, the $\delta_{\mathrm{LO_3}}$ is positive, and very close to the absolute value of $\delta_{\mathrm{LO_2}}$ plus a constant 12 (at 13 TeV) or 16 (at 100 TeV) percentage points. Moreover, even though also the $\delta_{\mathrm{NLO_2}}$ and $\delta_{\mathrm{NLO_3}}$ are depending quite strongly on the value of $m(t\bar{t}t\bar{t})$, they sum to almost a constant -1% (at 13 TeV) and -4% (at 100 TeV). Therefore, indeed, the entire sum $\mathrm{LO_2} + \mathrm{LO_3} + \mathrm{NLO_2} + \mathrm{NLO_3}$ is almost a constant 10% correction to the $\mathrm{LO_1} + \mathrm{NLO_1}$ — away from the threshold region.

In the threshold region, the situation is quite different. While the $\delta_{\mathrm{LO_3}}$ keeps increasing closer and closer to threshold, the derivative of $\delta_{\mathrm{LO_2}}$ reverses sign at $m(t\bar{t}t\bar{t}) \simeq 900\,\mathrm{GeV}$. In other words, the $\delta_{\mathrm{LO_2}}$ also starts to increase closer and closer to threshold. The same is true for the corrections induced by $\mathrm{NLO_2}$ and $\mathrm{NLO_3}$ contributions: the $\delta_{\mathrm{NLO_3}}$ sharply increases close to threshold. Hence, the delicate cancellation among the $\mathrm{LO_2}$ and $\mathrm{LO_3}$ (and

giving a correct picture. On top of this, from the inclusive results, we already know that there are also large cancellations between the $\mathrm{NLO_2}$ and $\mathrm{NLO_3}$ terms. Given the dominance of the gg-induced contributions, $\sum_{i=1}^{3} \mathrm{(N)LO}_i$ is already very close to the complete-NLO predictions, hence we show only the latter and compare them to the pure-QCD NLO predictions.

JHEP02(2018)031

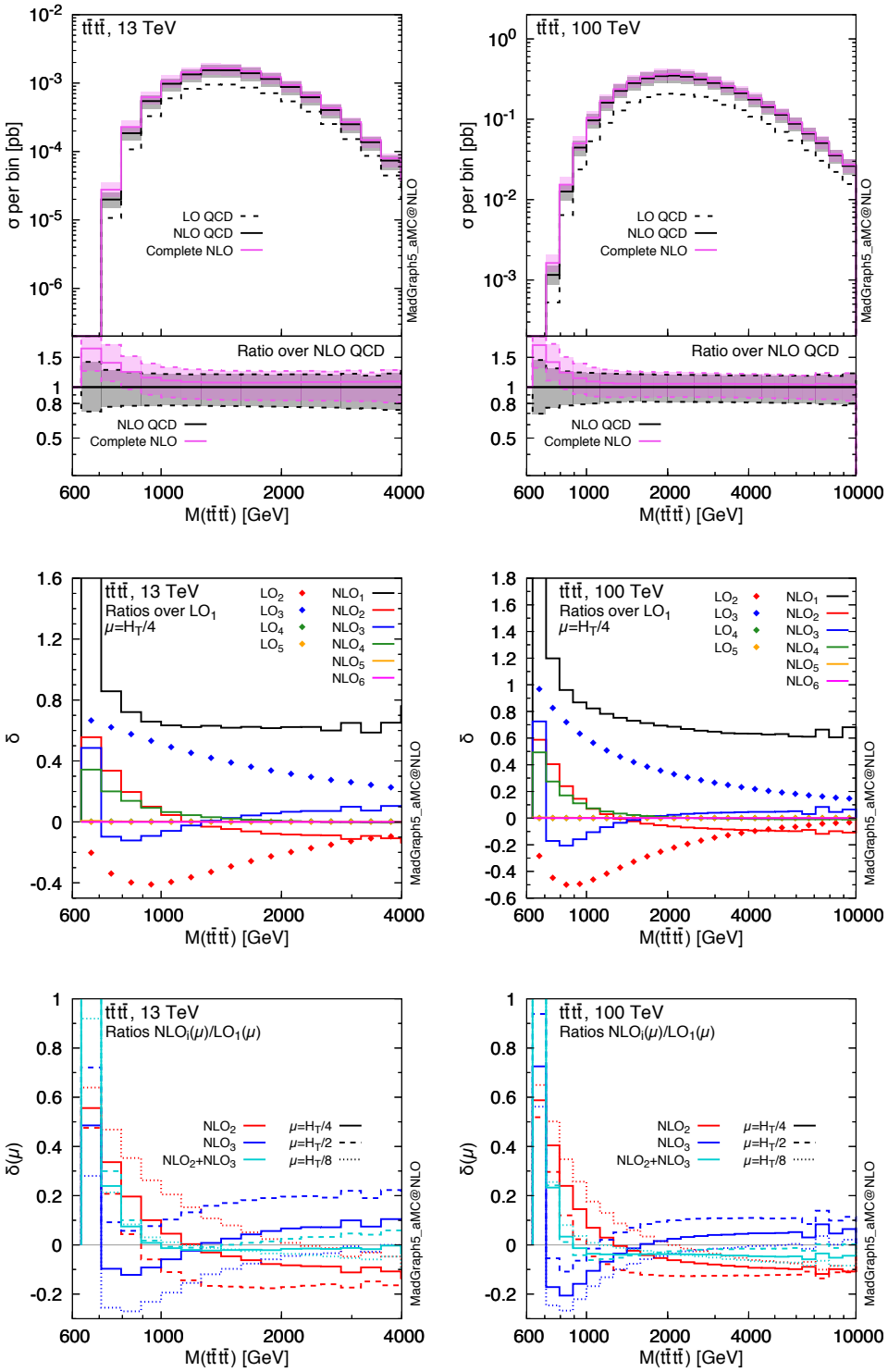

Figure 9. The $m(t\bar{t}t\bar{t})$ distribution in $t\bar{t}t\bar{t}$ production. Left: 13 TeV. Right: 100 TeV. Upper plots: scale uncertainty bands (same layout as the plots in figures 5 and 6). Central plots: individual (N)LO$_i$ contributions normalised to LO$_1 \equiv$ LO$_{\rm QCD}$. Lower plots: same as central plots but only with NLO$_2$, NLO$_3$, and their sum, at different values of the scale μ. These lower plots do not show scale uncertainties. Note that NLO$_1 \equiv$ NLO$_{\rm QCD}$ and NLO$_2 \equiv$ NLO$_{\rm EW}$.

JHEP02(2018)031

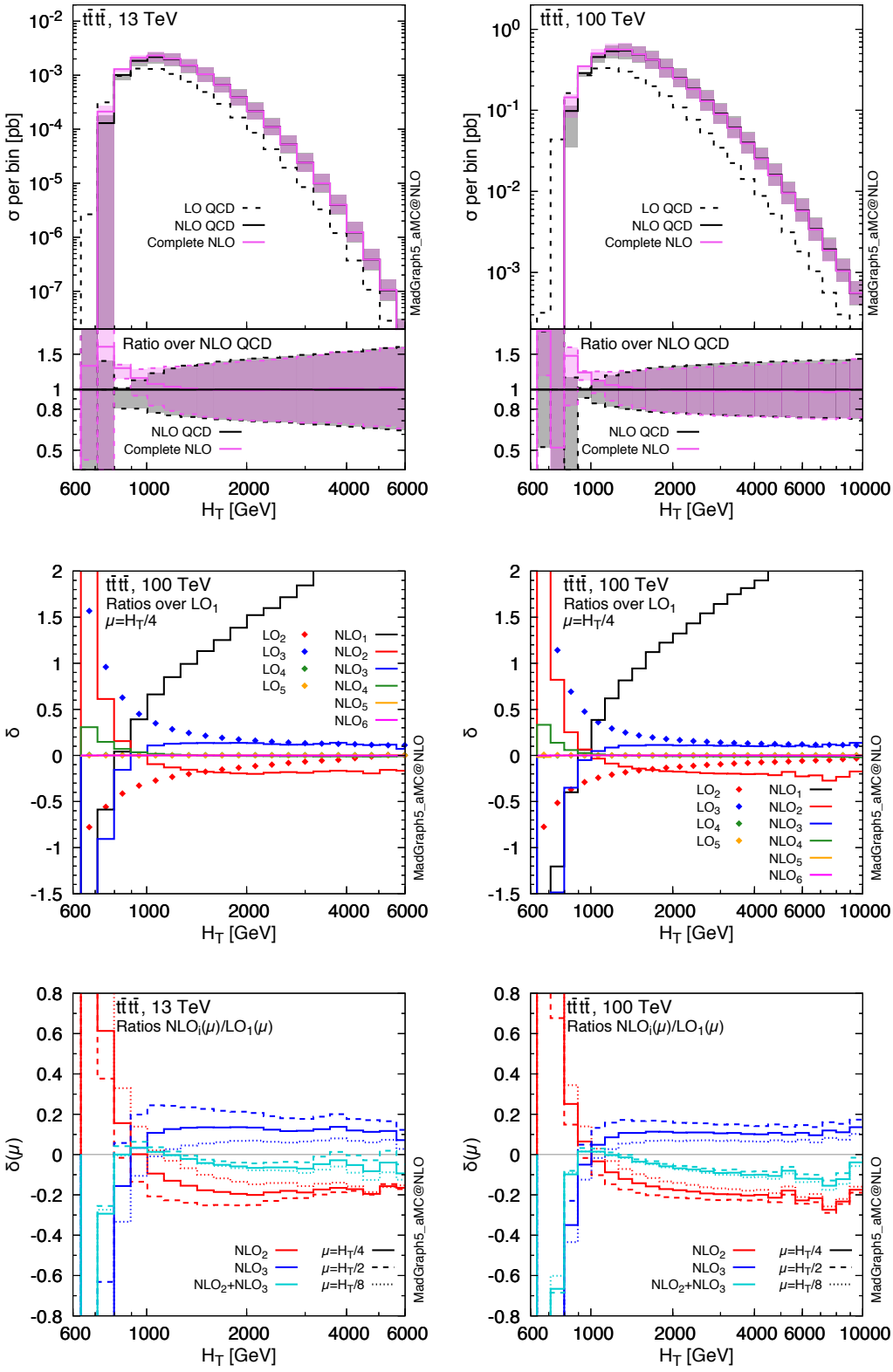

Figure 10. The H_T distribution in $t\bar{t}t\bar{t}$ production. See the caption of figure 9 for the description of the plots.

JHEP02(2018)031

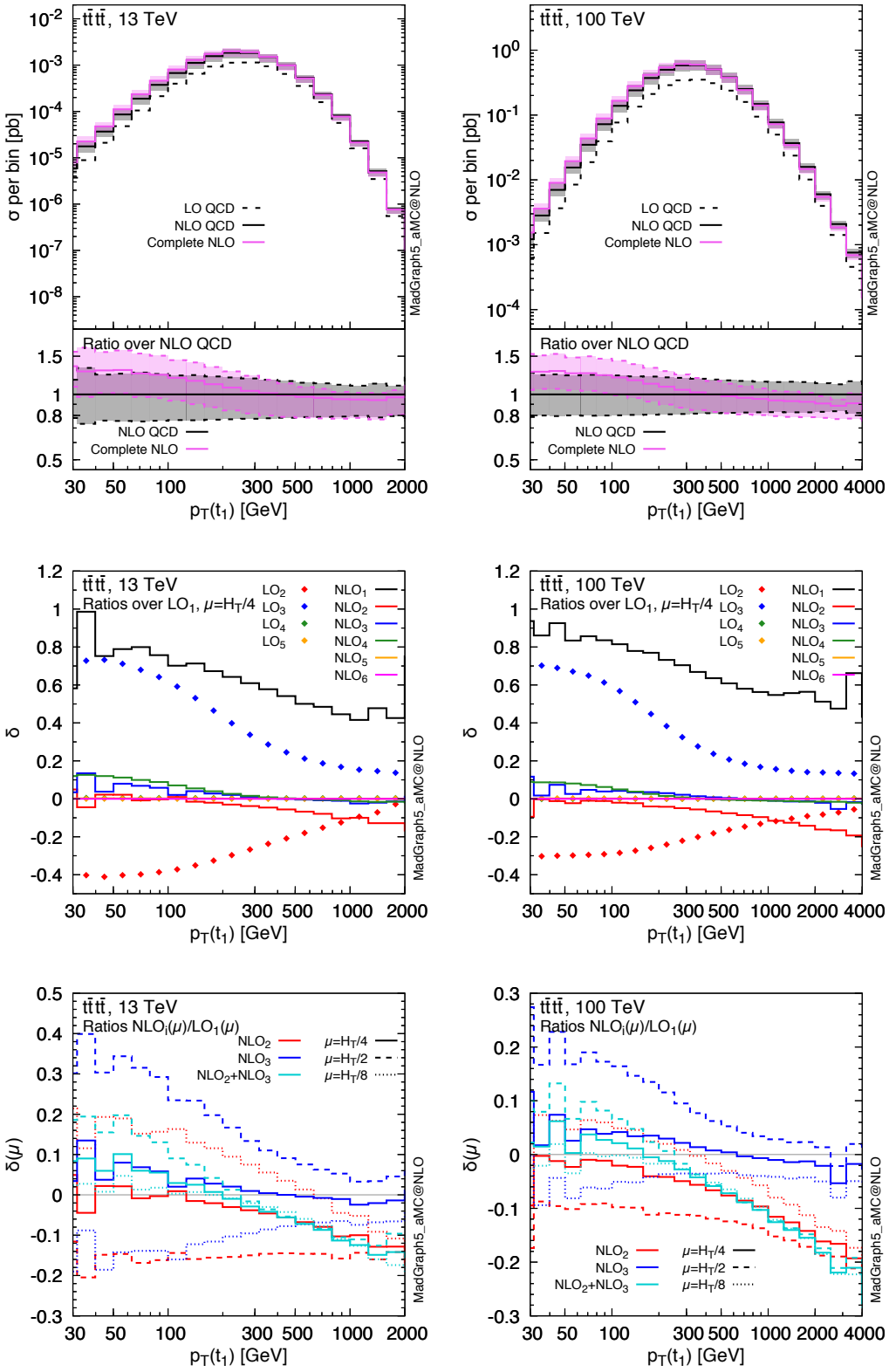

Figure 11. The $p_T(t_1)$ distribution in $t\bar{t}t\bar{t}$ production. See the caption of figure 9 for the description of the plots.

JHEP02(2018)031

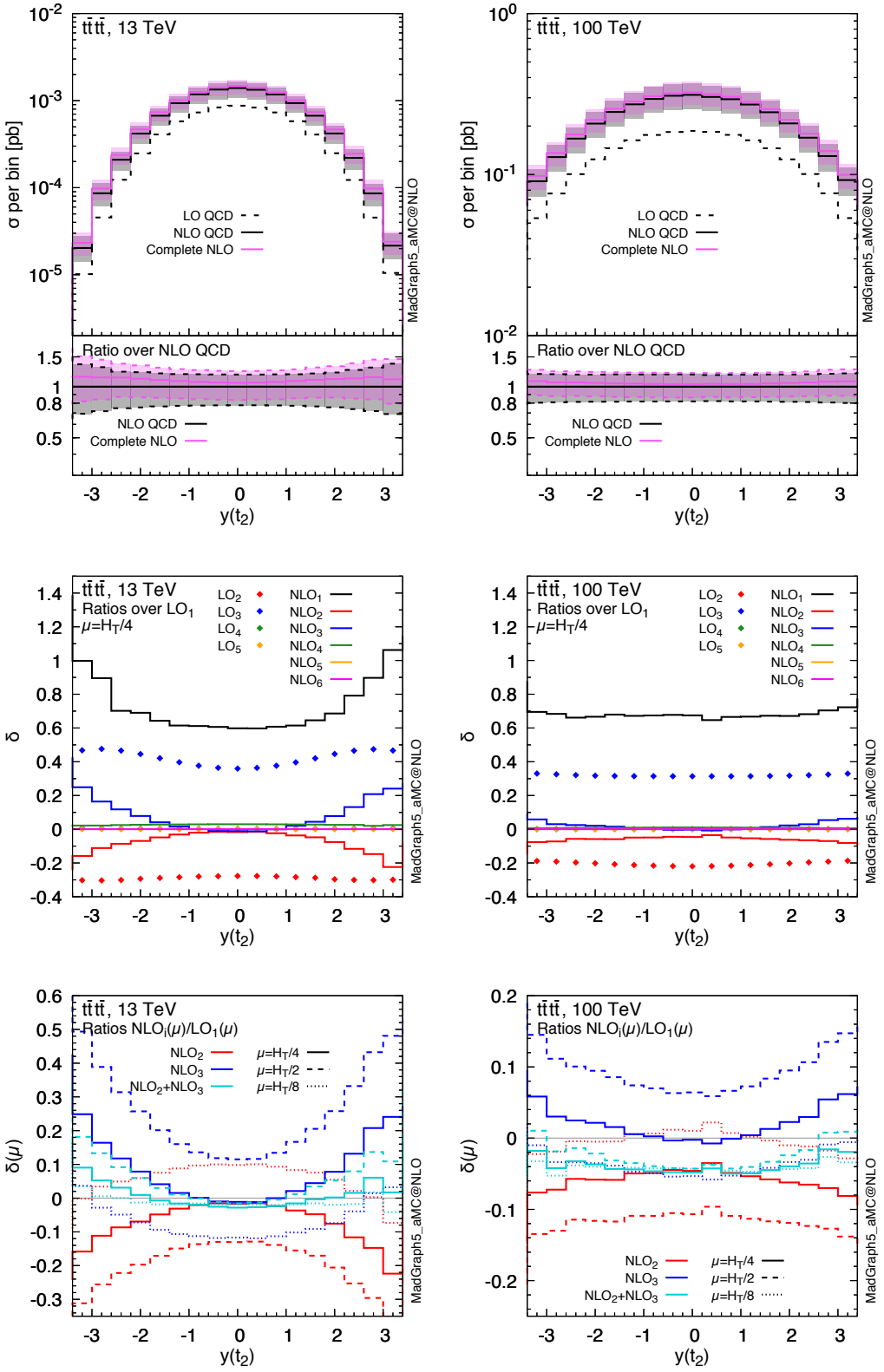

Figure 12. The $y(t_2)$ distribution in $t\bar{t}t\bar{t}$ production. See the caption of figure 9 for the description of the plots.

JHEP02(2018)031

NLO_2 and NLO_3) contributions completely breaks down in this region of phase space. Moreover, also the NLO_4 reaches several tens of percent close to threshold and should not be neglected when studying this region of phase space. Conversely, also at the differential level, LO_4, LO_5, NLO_5 and NLO_6 contributions are negligible.

There are two different physical effects at the origin of the large NLO corrections in the threshold region. First, also the LO_2 and LO_3 contributions are larger in this region and thus their "QCD corrections", which respectively enter the NLO_2 and NLO_3 contributions, preserve this increment w.r.t. the rest of the phase space. Second, the exchange of Z or Higgs bosons among top quarks, or in general among heavy particles, can lead to Sommerfeld enhancements when the top quarks are in a non-relativistic regime. This effect has already been documented in refs. [65, 66] for the case of top-quark pair production and in refs. [67–69] for the exchange of a virtual Higgs boson between an on-shell Higgs boson and another on-shell heavy particle. The threshold region forces each $t\bar{t}$, tt or $\bar{t}\bar{t}$ pair to potentially lead to this kind of effect. These large "EW corrections" on top of LO_1 and LO_2 terms lead to additional sizeable contributions to NLO_2 and NLO_3, respectively. Moreover, since also LO_3 is large, via this kind of "EW corrections" even NLO_4 is very large and incredibly enhanced w.r.t. the result at the inclusive level.

The lower plots in figure 9 further confirm the QCD origin of the NLO_2 and NLO_3 contributions. In order to explain this, we remind the reader that the scale dependence of the LO_2 and LO_3 contributions is the typical one, i.e., LO_2 and LO_3 absolute values become smaller when the scales are increased. In the plots we see that for NLO_3 the (dark blue) dashed lines are larger than the solid lines, which are in turn larger than dotted lines, while in the case of NLO_2 the order is the reversed. Since the LO_2 is negative, the NLO_2 term reduces the μ dependence of the LO_2 one and, similarly, the NLO_3 term reduces the μ dependence of the LO_3 one. Moreover, these plots confirm that also at the differential level there are large cancellations among the NLO_2 and NLO_3 terms and that the $\delta_{\mathrm{NLO}_2} + \delta_{\mathrm{NLO}_3}$ sum has a much smaller scale dependence than the two separate addends. In other words, the remarkable cancellations among the NLO_2 and NLO_3 corrections are not only present for the central value of μ, as already concluded from the middle plots in the discussion above, but also for their scale dependencies. Notably, these cancellations are present over a very large region of phase space. Also, if we had chosen, e.g., $H_T/2$ as our central scale (dashed lines in the lower plot), the NLO_2 and NLO_3 curves in the middle plots would have been much further apart, leading to much larger cancellations, since their sum would hardly have changed at all.

Compared to the invariant-mass distribution of the four tops, the case of the H_T distribution (figure 10) is similar in many respects. In particular, from the upper plots, we see that again only in the threshold region there is a sizeable difference between the NLO QCD predictions and the complete-NLO ones. It should be noted, though, that above the peak in the distribution, $H_T \gtrsim 1500\,\mathrm{GeV}$, the difference between the two predictions is very small, their central values as well as the scale uncertainties are lying almost exactly on top of each other. Just as in the case of the $m(t\bar{t}t\bar{t})$, the middle plots show that this is rather due to large and accidental cancellations among the various $(\mathrm{N})\mathrm{LO}_i$ with $i > 1$ contributions, which can individually reach several tens of percent.

JHEP02(2018)031

Close to the $H_T \simeq 4m_t$ threshold, the NLO_i contributions are in general reverted in sign w.r.t. the LO_i ones and receive particularly large enhancements in absolute value. This feature is due to large negative QCD Sudakov logarithms that appear in the limit $H_T \to 4m_t$. Indeed, since H_T includes in its definition the momentum of the possible extra jet, it effectively acts as a tight jet veto in this limit. Thus, "QCD corrections" involves large and negative contributions that have to be resummed. The effect is so large that in the first bin of the central plots of figure 10, the $\text{LO}_{\text{QCD}} + \text{NLO}_{\text{QCD}}$ prediction is negative and should not be trusted. This is a well-known instability of fixed-order perturbative calculations. Similar but smaller effects originate also from "EW corrections", due to the effective veto on the real emission.

It is also interesting to note how the μ-dependence of δ_{NLO_2} reduces for large values of H_T (see bottom plots of figure 10). We can see in the central plots that δ_{LO_2} is very small in this phase-space region, which means that the dominant NLO_2 contribution cannot be originated by "QCD corrections" on top of LO_2. Rather, it is mainly induced by "EW corrections" on top of the LO_{QCD} term. Thus, we recover the typical situation, which we found also in $t\bar{t}W^{\pm}$ production, where $\delta_{\text{NLO}_2} \equiv \delta_{\text{NLO}_{\text{EW}}}$ is almost independent of the value of μ.

An example of an observable in which the cancellation between the NLO_2 and NLO_3 is less complete in the whole range considered is the transverse momentum of the hardest of the two top quarks, shown in figure 11. Similarly to $m(t\bar{t}t\bar{t})$ and H_T, close to the threshold region, $p_T(t_1) \lesssim 300\,\text{GeV}$, the complete-NLO predictions are above the NLO QCD ones, reaching $\sim$25% at very small transverse momenta. On the other hand, for $p_T(t_1) \gtrsim 300\,\text{GeV}$, the complete-NLO corrections on top of the NLO QCD are growing negative and become about -10% in the tails of the distributions shown. From the middle plots, which refer to the case $\mu = H_T/4$, it becomes clear which orders are responsible for this behaviour. At small transverse momenta there are large positive corrections from the LO_3 (up to about 70% on top of LO_1) and to a lesser extent the NLO_4, which is itself slightly larger than NLO_3. LO_2 is also large, but negative, about -40% on top of LO_1, only partially cancelling the large positive contribution from LO_3. Accidentally, NLO_2 corrections are instead almost equal to zero.[12] Adding together all these contributions and taking also into account that the NLO_1 yields a positive 80% correction, we indeed find close to the threshold a correction of about 25% from complete-NLO result on top of the NLO QCD one. On the other hand, with increasing p_T, all the corrections quickly reduce (in absolute value), although not all in a uniform way. The exception is the δ_{NLO_2}, which steadily grows negative. Thus, at transverse momenta in the TeV range, the $\text{NLO}_2 \equiv \text{NLO}_{\text{EW}}$ becomes the dominant correction to the NLO QCD predictions. At first sight, this seems to be the standard situation with NLO EW corrections completely dominated by Sudakov logarithms, which we also observed in the NLO_2 curves for the $pp \to t\bar{t}W^{\pm}$ process, see figures 7 and 8. However, looking at the lower plots, it is clear that this cannot be the complete story. If the NLO_2 had been completely dominated by "EW corrections" on top of the LO_1, the δ_{NLO_2} ratio would have been (almost) scale independent. Conversely, although the scale

[12] Once again we want to remark that, unless differently specified, all the numbers in the main text refer to $\mu = H_T/4$, but they strongly depend on the scale μ. As can be seen from the lower plots, e.g., at 13 TeV for small transverse momenta $\delta_{\text{NLO}_2}(H_T/4) \sim 0\%$, but $\delta_{\text{NLO}_2}(H_T/8) \sim 20\%$ and $\delta_{\text{NLO}_2}(H_T/2) \sim -20\%$.

JHEP02(2018)031

dependence of δ_{NLO_2} does decrease with increasing transverse momenta, it remains anyway sizeable even in the far tail of the distribution. Therefore, a non-negligible part of NLO_2 is due to "QCD corrections" on top of the LO_2 also in the far tail. For these reasons, although in this phase-space region the individual and summed δ_{NLO_i} with $i > 1$ are not at all constant, the scale dependence of $\delta_{\text{NLO}_2} + \delta_{\text{NLO}_3}$ remains very small. The non-constant part seems to be the "EW corrections" entering the NLO_2, which are dominated by large and negative Sudakov logarithms and do not introduce a new scale dependence w.r.t. the LO_1.

From the $y(t_2)$ distribution (figure 12) we can see that, besides the threshold region, a non-negligible difference between NLO QCD and complete-NLO predictions is present also at 13 TeV (not 100 TeV) in the peripheral region of the softest of the top quark quarks. The $y(t_2)$ distribution is also the only one, among those considered, where the impact of the different (N)LO_i terms is qualitatively different at 13 and 100 TeV. While the LO_i corrections are rather flat at both 13 and 100 TeV, NLO_i corrections are flat only at 100 TeV; the NLO_i corrections for 13 TeV yield large effects in the peripheral region. The origin of this difference is the range of Bjorken-x probed in the PDFs, which is indeed very different at 13 and 100 TeV. While at 13 TeV the peripheral region is typically associated with tops that have large rapidities also in the $t\bar{t}t\bar{t}$ rest frame, at 100 TeV it is more likely that they originate from partonic initial states that are boosted w.r.t. the proton-proton reference frame.[13] For this reason the $y(t_2)$ distribution is flatter at 100 TeV than at 13 TeV, where large rapidities are strongly suppressed in a Born-like kinematics and therefore they are also much more sensitive to effects due to real emission from NLO_i contributions. However, as before, the NLO_2 and NLO_3 contributions almost cancel, resulting in at most $\sim$10% effects w.r.t. the LO_1 in the far forward and backward regions.

Given our findings, we suggest that the study of the μ-dependence of δ_{NLO_i} can be a very useful procedure for identifying the nature of NLO_i corrections in numerical calculations. For higher values of i, the $\Sigma_{\text{NLO}_i}(\mu)/\Sigma_{\text{LO}_{i-1}}(\mu)$ may be even more appropriate given the different numerical sizes of the LO_i terms and of their dependence on the running of α_s.[14] For instance, we verified that in $t\bar{t}t\bar{t}$ production both $\Sigma_{\text{NLO}_4}/\Sigma_{\text{LO}_3}$ and $\Sigma_{\text{NLO}_6}/\Sigma_{\text{LO}_5}$ are very mildly scale-dependent at inclusive and differential level. Indeed, both can be considered almost purely "EW corrections"; the latter by construction and the former due to the dominance of the gg initial-state. Conversely, we do not find this feature in the $\Sigma_{\text{NLO}_5}/\Sigma_{\text{LO}_4}$ ratio, since LO_4 and LO_5 contributions are both small but comparable in size and thus Σ_{NLO_5} receives large "QCD corrections" on top of LO_5 contributions.

In summary, at the inclusive and the differential levels complete-NLO results for $t\bar{t}t\bar{t}$ production are well within the NLO QCD uncertainties. For the observables presented here, there are no large qualitative differences between results at 13 and 100 TeV, except in the peripheral regions of the rapidity of the second hardest top quark. However, for all observables very large cancellations among the different perturbative orders are present both at the inclusive and differential level. Their individual sizes w.r.t. the LO_{QCD} prediction

[13] The maximum value for the rapidity of the $t\bar{t}t\bar{t}$ system in a Born-like configuration is $\log\left(\frac{13\text{ TeV}}{4m_t}\right) \sim 3$ at 13 TeV, while it is $\log\left(\frac{100\text{ TeV}}{4m_t}\right) \sim 5$ at 100 TeV.

[14] Note that $\Sigma_{\text{NLO}_i}/\Sigma_{\text{LO}_{i-1}} = \delta_{\text{NLO}_i}/\delta_{\text{LO}_{i-1}}$, so at the inclusive level the necessary information can be obtained from tables 7 and 8.

JHEP02(2018)031

are also strongly dependent on the scale definition. All these arguments point to the fact that in any BSM analysis involving $t\bar{t}t\bar{t}$ production contributions from all NLO corrections can be relevant. Thus, they should be taken into account, at least in the estimate of the theory uncertainty.

4 Conclusions

In this paper we have presented the complete-NLO predictions for $t\bar{t}W^{\pm}$ and $t\bar{t}t\bar{t}$ production at 13 and 100 TeV in proton-proton collisions. All the seven $\mathcal{O}(\alpha_s^i\alpha^j)$ contributions with $i+j=3,4$ and $j\geq 1$ for $t\bar{t}W^{\pm}$ production and all the eleven $\mathcal{O}(\alpha_s^i\alpha^j)$ contributions with $i+j=4,5$ have been calculated exactly without any approximation. We have shown that complete-NLO corrections involve large contributions beyond the NLO EW accuracy for both the $t\bar{t}W^{\pm}$ and $t\bar{t}t\bar{t}$ production processes

In $t\bar{t}W^{\pm}$ production we find that the $\mathcal{O}(\alpha_s\alpha^3)$ contributions, denoted as NLO_3 in this article, are larger than NLO EW corrections and have opposite sign. They are of the order 12(70)% of the LO at 13(100) TeV, with a strong dependence on particular kinematic variables such as $p_T(W^{\pm})$ and $p_T(t\bar{t})$, but not $m(t\bar{t})$. Thus, they are several orders of magnitude larger than the values naively expected from their coupling orders, i.e., $\text{NLO}_3/\text{LO} \gg \alpha^2/\alpha_s \sim 0.1\%$. The main reason is the opening of the $tW \to tW$ scattering in the NLO_3. Since the NLO QCD corrections are dominated by hard radiation, applying a jet veto suppresses the NLO_{QCD} contributions considerably. Conversely, the NLO_3 (and the NLO EW corrections) are affected to a much lesser extent, resulting in large corrections on top of the NLO-QCD result. At 13 TeV, applying a 100 GeV central jet veto, the central value of the complete-NLO prediction is typically outside the NLO QCD scale-uncertainty band. At 100 TeV, the uncertainty bands of these two predictions do not even touch. Besides their relevance for the SM and reliable comparisons with current and future measurements, these results further support the proposal of the BSM analysis described in ref. [33], showing a possible sensitivity to higher-dimensional operators in $tW \to tW$ scattering directly in $t\bar{t}W^{\pm}$ production. Rather than requiring a jet and considering $tW \to tW$ scattering as a Born process, our results suggest that the sensitivity may be increased by directly considering $t\bar{t}W^{\pm}$ production and vetoing additional jets.

In $t\bar{t}t\bar{t}$ production, LO contributions of $\mathcal{O}(\alpha_s^3\alpha)$ are about $-$25-30% of the purely-QCD $\mathcal{O}(\alpha_s^4)$ ones, while $\mathcal{O}(\alpha_s^2\alpha^2)$ contributions are about +30-45%, depending on the scale choice. For this reason, we find that the $\mathcal{O}(\alpha_s^4\alpha)$ (the NLO EW corrections, or NLO_2) as well as the $\mathcal{O}(\alpha_s^3\alpha^2)$ (denoted as NLO_3 in this article) contributions are also large. Moreover, since they receive large contributions from "QCD corrections" (and thus α_s and PDF renormalisation) on top of respectively $\mathcal{O}(\alpha_s^3\alpha)$ and $\mathcal{O}(\alpha_s^2\alpha^2)$ terms, they strongly depend on the scale definition. At 13 TeV, their relative impact w.r.t. purely-QCD $\mathcal{O}(\alpha_s^4)$ contribution varies in both cases between $\pm$15%. On the other hand, their sum reduces to a rather small $\pm$1-2%, and is almost independent from the QCD scale choice and kinematics. Qualitatively similar results are found also at 100 TeV. The size of the cancellations is quite remarkable, unexpected, and, to the best of our knowledge, accidental. Thus, a calculation of only part of the complete-NLO results would be missing important contributions. These

JHEP02(2018)031

large cancellations between the corrections and the reduced scale dependencies of their sum are not present very close to threshold. In this region of phase space, complete-NLO results are sizeably different from those at NLO QCD accuracy and even contributions of $\mathcal{O}(\alpha_s^2\alpha^3)$ (denoted as NLO_4 in this article) are found to be of the order of several tens of percents of the LO. Besides their relevance for the SM and reliable comparisons with current and future measurements, our calculations show that the possible impact of NLO corrections should be critically considered for studies such as ref. [34], where $t\bar{t}t\bar{t}$ production has been proposed as candidate, in conjunction with $t\bar{t}H$ production, for an independent determination of the Yukawa coupling of the top quark and the Higgs-boson total decay width. Similar considerations apply to other BSM studies involving $t\bar{t}t\bar{t}$ production: the various contributions from NLO corrections are large and the cancellations among them could be spoiled by BSM effects. This should be taken into account at least in the estimate of the theory uncertainties.

In this work we have also shown that the study of the μ-dependence of the quantity $\delta_{\text{NLO}_i} \equiv \Sigma_{\text{NLO}_i}(\mu)/\Sigma_{\text{LO}_1}(\mu)$ can be a very useful procedure for identifying the nature of NLO_i corrections in numerical calculations. A large scale dependence is a signal of "QCD corrections" on top of the LO_i contribution, while a scale independence for δ_{NLO_i} points to "EW corrections" on top of the LO_{i-1} contributions. For higher values of i, the $\Sigma_{\text{NLO}_i}(\mu)/\Sigma_{\text{LO}_{i-1}}(\mu)$ may be even more appropriate given the possible different numerical sizes of the LO_i terms and of their dependence on the running of α_s.

As a final remark, we want to remind the reader that the three known cases where NLO corrections from supposedly subleading EW contributions are large, $pp \to t\bar{t}W^{\pm}$, $pp \to t\bar{t}t\bar{t}$ and $pp \to W^+W^+jj$ with leptonic W^+ decays [26], involve very different mechanisms. In $t\bar{t}W^{\pm}$ production it is the opening of $tW \to tW$ scattering via the real emission in the NLO_3. In $t\bar{t}t\bar{t}$ production it is mainly the "QCD corrections" on top of EW $tt \to tt$ scattering, which gives large contributions already at the LO. In W^+W^+jj production it is instead the large EW Sudakov logarithmic corrections featured by the formally most subleading NLO contribution [27] together with the relatively large size (especially when standard VBS cuts are applied) of the purely EW W^+W^+ scattering component.

Acknowledgments

We are grateful to Hua-Sheng Shao, Stefano Frixione and Valentin Hirschi for the ongoing collaboration on the automation of the calculation of the complete-NLO corrections in the MadGraph5_aMC@NLO framework. We acknowledge Cen Zhang, Ennio Salvioni, Fabio Maltoni, Ioannis Tsinikos and Mathieu Pellen for enlightening discussions. The work of R.F. and D.P. is supported by the Alexander von Humboldt Foundation, in the framework of the Sofja Kovalevskaja Award Project "Event Simulation for the Large Hadron Collider at High Precision". The work of M.Z. has been supported by the Netherlands National Organisation for Scientific Research (NWO), by the European Union's Horizon 2020 research and innovation programme under the Marie Sklodovska-Curie grant agreement No 660171 and in part by the ILP LABEX (ANR-10-LABX-63), in turn supported by French state funds managed by the ANR within the "Investissements d'Avenir" programme under reference ANR-11-IDEX-0004-02.

JHEP02(2018)031

References

[1] J.M. Campbell and R.K. Ellis, *An update on vector boson pair production at hadron colliders*, *Phys. Rev.* **D 60** (1999) 113006 [hep-ph/9905386] [INSPIRE].

[2] G. Cullen et al., *Automated one-loop calculations with GoSam*, *Eur. Phys. J.* **C 72** (2012) 1889 [arXiv:1111.2034] [INSPIRE].

[3] G. Cullen et al., *GoSam-2.0: a tool for automated one-loop calculations within the Standard Model and beyond*, *Eur. Phys. J.* **C 74** (2014) 3001 [arXiv:1404.7096] [INSPIRE].

[4] S. Badger, B. Biedermann, P. Uwer and V. Yundin, *Numerical evaluation of virtual corrections to multi-jet production in massless QCD*, *Comput. Phys. Commun.* **184** (2013) 1981 [arXiv:1209.0100] [INSPIRE].

[5] F. Cascioli, P. Maierhofer and S. Pozzorini, *Scattering amplitudes with open loops*, *Phys. Rev. Lett.* **108** (2012) 111601 [arXiv:1111.5206] [INSPIRE].

[6] S. Actis, A. Denner, L. Hofer, A. Scharf and S. Uccirati, *Recursive generation of one-loop amplitudes in the Standard Model*, *JHEP* **04** (2013) 037 [arXiv:1211.6316] [INSPIRE].

[7] S. Actis, A. Denner, L. Hofer, J.-N. Lang, A. Scharf and S. Uccirati, *RECOLA: REcursive Computation of One-Loop Amplitudes*, *Comput. Phys. Commun.* **214** (2017) 140 [arXiv:1605.01090] [INSPIRE].

[8] T. Gleisberg et al., *Event generation with SHERPA 1.1*, *JHEP* **02** (2009) 007 [arXiv:0811.4622] [INSPIRE].

[9] G. Bevilacqua et al., *HELAC-NLO*, *Comput. Phys. Commun.* **184** (2013) 986 [arXiv:1110.1499] [INSPIRE].

[10] V. Hirschi, R. Frederix, S. Frixione, M.V. Garzelli, F. Maltoni and R. Pittau, *Automation of one-loop QCD corrections*, *JHEP* **05** (2011) 044 [arXiv:1103.0621] [INSPIRE].

[11] J. Alwall et al., *The automated computation of tree-level and next-to-leading order differential cross sections and their matching to parton shower simulations*, *JHEP* **07** (2014) 079 [arXiv:1405.0301] [INSPIRE].

[12] S. Alioli, P. Nason, C. Oleari and E. Re, *A general framework for implementing NLO calculations in shower Monte Carlo programs: the POWHEG BOX*, *JHEP* **06** (2010) 043 [arXiv:1002.2581] [INSPIRE].

[13] S. Platzer and S. Gieseke, *Dipole showers and automated NLO matching in HERWIG++*, *Eur. Phys. J.* **C 72** (2012) 2187 [arXiv:1109.6256] [INSPIRE].

[14] S. Kallweit, J.M. Lindert, P. Maierhöfer, S. Pozzorini and M. Schönherr, *NLO electroweak automation and precise predictions for W + multijet production at the LHC*, *JHEP* **04** (2015) 012 [arXiv:1412.5157] [INSPIRE].

[15] S. Kallweit, J.M. Lindert, P. Maierhofer, S. Pozzorini and M. Schönherr, *NLO QCD+EW predictions for V + jets including off-shell vector-boson decays and multijet merging*, *JHEP* **04** (2016) 021 [arXiv:1511.08692] [INSPIRE].

JHEP02(2018)031

[16] B. Biedermann, S. Bräuer, A. Denner, M. Pellen, S. Schumann and J.M. Thompson, *Automation of NLO QCD and EW corrections with Sherpa and Recola*, *Eur. Phys. J.* **C 77** (2017) 492 [arXiv:1704.05783] [INSPIRE].

[17] S. Frixione, V. Hirschi, D. Pagani, H.S. Shao and M. Zaro, *Weak corrections to Higgs hadroproduction in association with a top-quark pair*, *JHEP* **09** (2014) 065 [arXiv:1407.0823] [INSPIRE].

[18] S. Frixione, V. Hirschi, D. Pagani, H.S. Shao and M. Zaro, *Electroweak and QCD corrections to top-pair hadroproduction in association with heavy bosons*, *JHEP* **06** (2015) 184 [arXiv:1504.03446] [INSPIRE].

[19] R. Frederix, S. Frixione, V. Hirschi, D. Pagani, H.-S. Shao and M. Zaro, *The complete NLO corrections to dijet hadroproduction*, *JHEP* **04** (2017) 076 [arXiv:1612.06548] [INSPIRE].

[20] M. Chiesa, N. Greiner and F. Tramontano, *Automation of electroweak corrections for LHC processes*, *J. Phys.* **G 43** (2016) 013002 [arXiv:1507.08579] [INSPIRE].

[21] N. Greiner and M. Schönherr, *NLO QCD+EW corrections to diphoton production in association with a vector boson*, *JHEP* **01** (2018) 079 [arXiv:1710.11514] [INSPIRE].

[22] G. Heinrich, *QCD calculations for the LHC: status and prospects*, arXiv:1710.04998 [INSPIRE].

[23] C. Anastasiou, C. Duhr, F. Dulat, F. Herzog and B. Mistlberger, *Higgs boson gluon-fusion production in QCD at three loops*, *Phys. Rev. Lett.* **114** (2015) 212001 [arXiv:1503.06056] [INSPIRE].

[24] F.A. Dreyer and A. Karlberg, *Vector-boson fusion Higgs production at three loops in QCD*, *Phys. Rev. Lett.* **117** (2016) 072001 [arXiv:1606.00840] [INSPIRE].

[25] M. Czakon, D. Heymes, A. Mitov, D. Pagani, I. Tsinikos and M. Zaro, *Top-pair production at the LHC through NNLO QCD and NLO EW*, *JHEP* **10** (2017) 186 [arXiv:1705.04105] [INSPIRE].

[26] B. Biedermann, A. Denner and M. Pellen, *Complete NLO corrections to W^+W^+ scattering and its irreducible background at the LHC*, *JHEP* **10** (2017) 124 [arXiv:1708.00268] [INSPIRE].

[27] B. Biedermann, A. Denner and M. Pellen, *Large electroweak corrections to vector-boson scattering at the Large Hadron Collider*, *Phys. Rev. Lett.* **118** (2017) 261801 [arXiv:1611.02951] [INSPIRE].

[28] CMS collaboration, *Measurement of top pair-production in association with a W or Z boson in pp collisions at* 13 *TeV*, CMS-PAS-TOP-17-005, CERN, Geneva Switzerland, (2017).

[29] ATLAS collaboration, *Measurement of the $t\bar{t}Z$ and $t\bar{t}W$ production cross sections in multilepton final states using* 3.2 fb^{-1} *of pp collisions at* $\sqrt{s} = 13$ *TeV with the ATLAS detector*, *Eur. Phys. J.* **C 77** (2017) 40 [arXiv:1609.01599] [INSPIRE].

[30] CMS collaboration, *Search for the Standard Model production of four top quarks with same-sign and multilepton final states in proton-proton collisions at* $\sqrt{s} = 13$ *TeV*, CMS-PAS-TOP-17-009, CERN, Geneva Switzerland, (2017).

[31] J.R. Andersen et al., *Les Houches* 2015*: physics at TeV colliders Standard Model working group report*, in 9$^{\text{th}}$ *Les Houches Workshop on Physics at TeV Colliders (PhysTeV* 2015*)*, Les Houches France, 1–19 June 2015 [arXiv:1605.04692] [INSPIRE].

[32] R. Frederix, S. Frixione, V. Hirschi, D. Pagani, H.-S. Shao and M. Zaro, in preparation.

[33] J.A. Dror, M. Farina, E. Salvioni and J. Serra, *Strong tW scattering at the LHC*, *JHEP* **01** (2016) 071 [arXiv:1511.03674] [INSPIRE].

JHEP02(2018)031

[34] Q.-H. Cao, S.-L. Chen and Y. Liu, *Probing Higgs width and top quark Yukawa coupling from $t\bar{t}H$ and $t\bar{t}t\bar{t}$ productions*, *Phys. Rev.* **D 95** (2017) 053004 [arXiv:1602.01934] [INSPIRE].

[35] M.V. Garzelli, A. Kardos, C.G. Papadopoulos and Z. Trócsányi, *$t\bar{t}W^{\pm}$ and $t\bar{t}Z$ hadroproduction at NLO accuracy in QCD with parton shower and hadronization effects*, *JHEP* **11** (2012) 056 [arXiv:1208.2665] [INSPIRE].

[36] J.M. Campbell and R.K. Ellis, *$t\bar{t}W^{\pm}$ production and decay at NLO*, *JHEP* **07** (2012) 052 [arXiv:1204.5678] [INSPIRE].

[37] F. Maltoni, M.L. Mangano, I. Tsinikos and M. Zaro, *Top-quark charge asymmetry and polarization in $t\bar{t}W^{\pm}$ production at the LHC*, *Phys. Lett.* **B 736** (2014) 252 [arXiv:1406.3262] [INSPIRE].

[38] F. Maltoni, D. Pagani and I. Tsinikos, *Associated production of a top-quark pair with vector bosons at NLO in QCD: impact on $t\bar{t}H$ searches at the LHC*, *JHEP* **02** (2016) 113 [arXiv:1507.05640] [INSPIRE].

[39] H.T. Li, C.S. Li and S.A. Li, *Renormalization group improved predictions for $t\bar{t}W^{\pm}$ production at hadron colliders*, *Phys. Rev.* **D 90** (2014) 094009 [arXiv:1409.1460] [INSPIRE].

[40] A. Broggio, A. Ferroglia, G. Ossola and B.D. Pecjak, *Associated production of a top pair and a W boson at next-to-next-to-leading logarithmic accuracy*, *JHEP* **09** (2016) 089 [arXiv:1607.05303] [INSPIRE].

[41] A. Kulesza, L. Motyka, D. Schwartländer, T. Stebel and V. Theeuwes, *Soft gluon resummation for the associated production of a top quark pair with a W boson at the LHC*, arXiv:1710.06810 [INSPIRE].

[42] LHC Higgs Cross section Working Group collaboration, D. de Florian et al., *Handbook of LHC Higgs cross sections: 4. Deciphering the nature of the Higgs sector*, arXiv:1610.07922 [INSPIRE].

[43] G. Bevilacqua and M. Worek, *Constraining BSM physics at the LHC: four top final states with NLO accuracy in perturbative QCD*, *JHEP* **07** (2012) 111 [arXiv:1206.3064] [INSPIRE].

[44] S. Frixione, Z. Kunszt and A. Signer, *Three jet cross-sections to next-to-leading order*, *Nucl. Phys.* **B 467** (1996) 399 [hep-ph/9512328] [INSPIRE].

[45] S. Frixione, *A general approach to jet cross-sections in QCD*, *Nucl. Phys.* **B 507** (1997) 295 [hep-ph/9706545] [INSPIRE].

[46] R. Frederix, S. Frixione, F. Maltoni and T. Stelzer, *Automation of next-to-leading order computations in QCD: the FKS subtraction*, *JHEP* **10** (2009) 003 [arXiv:0908.4272] [INSPIRE].

[47] R. Frederix, S. Frixione, A.S. Papanastasiou, S. Prestel and P. Torrielli, *Off-shell single-top production at NLO matched to parton showers*, *JHEP* **06** (2016) 027 [arXiv:1603.01178] [INSPIRE].

[48] G. Ossola, C.G. Papadopoulos and R. Pittau, *Reducing full one-loop amplitudes to scalar integrals at the integrand level*, *Nucl. Phys.* **B 763** (2007) 147 [hep-ph/0609007] [INSPIRE].

[49] P. Mastrolia, E. Mirabella and T. Peraro, *Integrand reduction of one-loop scattering amplitudes through Laurent series expansion*, *JHEP* **06** (2012) 095 [*Erratum ibid.* **11** (2012) 128] [arXiv:1203.0291] [INSPIRE].

[50] G. Passarino and M.J.G. Veltman, *One loop corrections for e^+e^- annihilation into $\mu^+\mu^-$ in the Weinberg model*, *Nucl. Phys.* **B 160** (1979) 151 [INSPIRE].

JHEP02(2018)031

[51] A.I. Davydychev, *A simple formula for reducing Feynman diagrams to scalar integrals*, *Phys. Lett.* **B 263** (1991) 107 [INSPIRE].

[52] A. Denner and S. Dittmaier, *Reduction schemes for one-loop tensor integrals*, *Nucl. Phys.* **B 734** (2006) 62 [hep-ph/0509141] [INSPIRE].

[53] G. Ossola, C.G. Papadopoulos and R. Pittau, *CutTools: a program implementing the OPP reduction method to compute one-loop amplitudes*, *JHEP* **03** (2008) 042 [arXiv:0711.3596] [INSPIRE].

[54] T. Peraro, *Ninja: automated integrand reduction via Laurent expansion for one-loop amplitudes*, *Comput. Phys. Commun.* **185** (2014) 2771 [arXiv:1403.1229] [INSPIRE].

[55] V. Hirschi and T. Peraro, *Tensor integrand reduction via Laurent expansion*, *JHEP* **06** (2016) 060 [arXiv:1604.01363] [INSPIRE].

[56] A. Denner, S. Dittmaier and L. Hofer, *COLLIER: a fortran-based Complex One-Loop LIbrary in Extended Regularizations*, *Comput. Phys. Commun.* **212** (2017) 220 [arXiv:1604.06792] [INSPIRE].

[57] A. Manohar, P. Nason, G.P. Salam and G. Zanderighi, *How bright is the proton? A precise determination of the photon parton distribution function*, *Phys. Rev. Lett.* **117** (2016) 242002 [arXiv:1607.04266] [INSPIRE].

[58] A.V. Manohar, P. Nason, G.P. Salam and G. Zanderighi, *The photon content of the proton*, *JHEP* **12** (2017) 046 [arXiv:1708.01256] [INSPIRE].

[59] J. Butterworth et al., *PDF4LHC recommendations for LHC run II*, *J. Phys.* **G 43** (2016) 023001 [arXiv:1510.03865] [INSPIRE].

[60] NNPDF collaboration, R.D. Ball et al., *Parton distributions for the LHC run II*, *JHEP* **04** (2015) 040 [arXiv:1410.8849] [INSPIRE].

[61] L.A. Harland-Lang, A.D. Martin, P. Motylinski and R.S. Thorne, *Parton distributions in the LHC era: MMHT* 2014 *PDFs*, *Eur. Phys. J.* **C 75** (2015) 204 [arXiv:1412.3989] [INSPIRE].

[62] S. Dulat et al., *New parton distribution functions from a global analysis of quantum chromodynamics*, *Phys. Rev.* **D 93** (2016) 033006 [arXiv:1506.07443] [INSPIRE].

[63] M.L. Mangano et al., *Physics at a* 100 *TeV pp collider: Standard Model processes*, *CERN Yellow Report* (2017) 1 [arXiv:1607.01831] [INSPIRE].

[64] C. Zhang, *Constraining qqtt operators from four-top production: a case for enhanced EFT sensitivity*, arXiv:1708.05928 [INSPIRE].

[65] J.H. Kühn, A. Scharf and P. Uwer, *Weak interactions in top-quark pair production at hadron colliders: an update*, *Phys. Rev.* **D 91** (2015) 014020 [arXiv:1305.5773] [INSPIRE].

[66] M. Beneke, A. Maier, J. Piclum and T. Rauh, *Higgs effects in top anti-top production near threshold in e^+e^- annihilation*, *Nucl. Phys.* **B 899** (2015) 180 [arXiv:1506.06865] [INSPIRE].

[67] G. Degrassi, P.P. Giardino, F. Maltoni and D. Pagani, *Probing the Higgs self coupling via single Higgs production at the LHC*, *JHEP* **12** (2016) 080 [arXiv:1607.04251] [INSPIRE].

[68] W. Bizon, M. Gorbahn, U. Haisch and G. Zanderighi, *Constraints on the trilinear Higgs coupling from vector boson fusion and associated Higgs production at the LHC*, *JHEP* **07** (2017) 083 [arXiv:1610.05771] [INSPIRE].

[69] F. Maltoni, D. Pagani, A. Shivaji and X. Zhao, *Trilinear Higgs coupling determination via single-Higgs differential measurements at the LHC*, *Eur. Phys. J.* **C 77** (2017) 887 [arXiv:1709.08649] [INSPIRE].

JHEP02(2018)031